

Change of lithofacies in marine sediment core from Quaternary to Pre-Quaternary: A case study from the Central Indian Ocean Basin

SimontiniSensarma*¹, ShyamM. Gupta¹, Ranadip Banerjee¹ and Subir Mukhopadhyay²

¹Geological Oceanography Division, CSIR-National Institute of Oceanography,
Dona Paula, Goa - 403004

²Department of Geological Sciences, Jadavpur University, Kolkata - 700032

*Corresponding author, email: simontinisensarma@gmail.com

Abstract

A distinct change in lithofacies was observed from red clay to siliceous ooze in a core from Indian Ocean. Radiolarian index species were used to ascertain the Quaternary datum levels and an age of 2.0Ma is determined up to 125cm depth from surface. Below 185cm depth, the sediment core lacked radiolarian test completely. At about 50cm from core top, the sedimentation rate decreased drastically from 0.18 to 0.05cm/kyr with a corresponding age of 500kyr, marking Marine Isotope Stage 13. The changes in lithofacies and sedimentation rate are further accompanied by the change in clay mineralogy from smectite rich older sediments to smectite depleted younger sediments and presence of higher amount of volcanogenic materials in the older sediments. Higher values of Chemical Index of Alteration and lower K_2O/Al_2O_3 in older sediments indicate dominance of chemical weathering in the older sediments which decreased gradually towards core top. Ti normalized concentrations of elements like Co, V, Cu, Ni, Ce, Y and $\sum REEs$ exhibit lowest values at the transition zone above which the ratios increased steadily towards the core top. All these observations indicate a marked change in the climatic regime from late Quaternary onwards, prior to which the environment was less bio-productive.

Keywords: Indian Ocean; sediment core; biostratigraphy; clay minerals; geochemistry.

1. Introduction

The study of stratigraphic successions of terrestrial basins is comparatively easier than modern-day deep-sea basins due to inaccessibility of the study area and inadequate sample size of the latter. Few of the best ways to identify stratigraphic changes in marine-sediment records is by identifying the discontinuity surfaces that can be ascertained by a change in lithology, surface morphology, biological activity, mineralization, facies contrasts or diagenetic contrast between underlying and overlying units (Brady and Bowie, 2017). The documentation of such discontinuity surfaces unveils important tectonic and eustatic processes, which are again caused by regional and local environmental changes (Hillgärtner, 1998). Discontinuity surfaces (or discontinuities) are of interest due to their importance in resolving high-frequency sea-level fluctuations and basin evolution at scales finer than chronostratigraphic resolution typically available (Hillgärtner, 1998; Christ *et al.*, 2012; Brady and Bowie, 2017). In the Indian Ocean scenario, various works have been done on aspects like biostratigraphy, hydrothermal/volcanogenic signatures, bulk geochemistry and mineralogy of sediment cores, particularly in the Central Indian Ocean Basin (CIOB), due to its increased importance during late 90's when vast deposits of polymetallic nodules were found in this basin.

The radiolarian zonation of Quaternary sediments from the CIOB has been done by Gupta (1988). Banakar *et al.*, (1991) and Borole (1993) have shown with the help of radiochemical and radiolarian data respectively how Antarctic Bottom Water (AABW) has been instrumental in eroding the surface sediments of the CIOB and enriching them with transition metals like manganese, nickel, copper etc. possibly due to higher dissolved oxygen during glacial conditions. Iyer *et al.*, (1997), Sukumaran *et al.*, (1999) and Pereira *et al.*, (2006) have shown the possibility of an *in situ* volcanogenic/hydrothermal activity in the CIOB by comparing the morpho-chemical data of glass shards found from both the CIOB and the Indonesian Arc Volcanism (IAV). Role of micronodules in controlling REE distribution in a sediment column has been discussed by Pattan and Banakar (1997) whereas, mineralogy of different size fraction and their implication on climatic control has been discussed by Nath *et al.*, (2005). On the other hand, bulk geochemistry of the CIOB sediment cores has been studied by Mudholkar *et al.*, (1993) and Pattan *et al.*, (2005) among others. In a recent work by Nath *et al.*, (2013), a good agreement between the ages dated by various methods (radiolarian and coccolith index species, $^{230}\text{Th}_{\text{excess}}$, and AMS ^{14}C) is shown and the influence of Mid-Brunhes climatic event in the sediment record of the CIOB is also reported. Off shore Australia, a core spanning 550kyr with continuous sedimentation has been reported to have warmer inter glacials and drier glacials during mid to late Quaternary due to meridional shifts in the

atmospheric circulation system (Stuut *et al.*, 2014). However, all these studies target a single, mostly local phenomenon and fails to give an insight into the changes encountered in a marine environment through time. Thus, in the present study, new geochemical, mineralogical and biological data has been presented from a sediment core in the CIOB and from their inter relationship a comprehensive picture about the varying depositional condition in that area has been ascertained.

2. Materials and Method:

2.1. Study area and sampling:

A 5.4m long sediment core (AAS-38/4) was collected at a water depth of 4935m from the siliceous sediment of the CIOB (13°59.76'S; 74°59.74'E) during the 38th cruise of AA Sidorenko. After collection, the entire core was sub-sampled at 5cm interval, washed thoroughly with deionized water, dried and packed in air tight zip lock bags and stored in screw cap plastic containers at room temperature. The location of the core is given in Fig 1.

2.2. Coarse fraction observation and biostratigraphic slide preparation:

Each section of the core (107 sub-sections) were wet sieved by 63µm mesh to separate the sand sized particles, to identify the coarse fraction (CF) content of the sediment under an Olympus SZX7 stereo-zoom Microscope. Hand-picked CF components were also observed under a Scanning Electron Microscopic (SEM) using a JEOL JSM-5800LV SEM, operating at 20kV, 55nA and were focused (3–5µm) (Pereira *et al.*, 2006; Iyer *et al.*, 2012). The main components of the CF were radiolarian tests, glass shards, pumice, palagonite crystals, micronodules, plagioclase, quartz and other rock fragments and some zeolite crystals. Sediment samples were taken at ~25cm interval and processed for the radiolarian biostratigraphy following strewn slides method (Nigrini, 1971; Gupta, 1988). The yields of the sieved sediments (radiolarian tests) were strewn on to glass slides on a hot plate and after drying, the permanent mounts were made.

2.3. Clay mineralogy identification:

The clay fraction (<2µm) was separated by the settling technique according to Stokes' law (Folk, 1968) from the silt+clay fraction (<63µm). Inorganic and organic carbon contents of the sediment were removed by treating them with acetic acid and hydrogen peroxide respectively. After that, the samples were repeatedly washed with deionized water to remove the trace of acetic acid, peroxide and salt. Thick slurry of sediments was then prepared and pipetted onto glass slides, glycolated overnight at 60°C, and kept in the desiccators (Nath *et al.*, 2013). Just before the analysis they were

taken out and brought to room temperature while still inside the desiccators. The clay mineralogy was carried out with an X-ray diffractometer (Rigaku – Ultima IV) using nickel filtered Cu K α radiation operated at 40kV power and 20mA current, from 3-32° range and at a speed of 20min⁻¹.

2.4. Major element analysis:

Splits of each samples (0.55g) were fused into borate glass beads at high temperature (1180°C) using Spectromelt® A12, Merck. The detail description of the procedure has been described in Ray *et al.*, (2014). These beads were then analyzed for the determination of major element oxide by using X-Ray Fluorescence Spectrometer (PANalytical, AXIOS®). Marine sediment reference JSd-1 was used as standard and details of the analysis is given in Table 3.

2.5 Trace and Rare Earth element (REE) analysis:

The bulk trace and REE concentrations were measured by an X-Series II (Thermo Fisher) quadrupole Inductively Coupled Plasma-Mass Spectrometer (ICP-MS) after complete digestion of the samples (50mg each) with acid mixture HF:HNO₃:HClO₄ in the ratio 7:3:1 (Pattan *et al.*, 2013). After complete digestion of the samples, 4ml (1:1) supra-pure nitric acid solution was added to them and transferred into 100ml volumetric flask. An internal standard of ¹⁰³Rh solution (1ng/ml) was added to each of them and volume was made upto 100ml with Milli-Q water. Marine sediment reference JSd-1 was used as standard and details of the analysis is given in Table 3.

3. Results:

3.1. Physical characteristics of the sediments:

From the core top, upto 180-185cm interval, the sediments are pale yellow to brownish in colour. More than 90% of the CF components are radiolarian tests (Fig 2a and b) which made the sediment porous and light in nature. Below 180-185cm section, the sediments are composed of mainly dark reddish brown coloured, compact clay. The CF percentage markedly diminished due to disappearance of radiolarian tests below 125cm and the main component became palagonite crystals (Fig 2c). Yellowish orange to brown coloured palagonites are found in the present study, with average dimension of 0.16-0.25mm. Glass shards are ubiquitous throughout the core in varying proportions, ranging from platy ones, blocky types to even bubble walled types (Fig 2d). They are transparent, irregular in habit without any abrasion or rounded edges, indicating that they are not much reworked. Their abundance varied from <1% up to 18.7% of the total CF content in certain sub-sections with an average dimension of 0.12mm. Pumice, a type of rock consisting of highly vesicular rough textured volcanic glass, is also observed in some sections. They are generally off white to pink in colour, 0.25-1mm long and are sometimes attached with radiolaria and

micronodules. Alteration of pumice to palagonite is observed 185cm afterwards. Quartz and plagioclase grains are found almost throughout the entire length of the core. The average grain sizes of the quartz and plagioclase crystals are like that of the glass shards. Micronodules also constituted a part of the CF, which are basically tiny concretionary bodies of iron-manganese oxides (Fig 2e). Their abundance varied from <1% upto 35% of the total CF population and are 0.08mm long. Most of them are botryoidal in habit and are seen to be attached with the radiolarian tests, pumice and palagonite. Zeolites are observed in few sub-sections, viz. 145-150cm, 155-165cm, 305-310cm and 525-530cm with an average concentration of 10% of total CF population (Fig 2f). They are whitish to transparent with acicular, needle like crystals, radiating from a point and often associated with the pumice and radiolarian tests. Their physical appearance is similar to natrolite and have average dimension of 0.1mm.

3.2. Clay mineralogy:

The down-core variation of clay mineralogy is presented in Fig 3. A distinct change in the bulk clay mineral composition is observed in the core. From the core top, up to 70cm depth, prominent peaks of kaolinite and chlorite are obtained at 7.14Å. A lesser prominent peak of illite is obtained at 9.7Å (Fig 3a). Kaolinite also showed a separate peak at 3.57Å, but no smectite peak is observed till 70cm core depth. Illite and chlorite are mostly derived from land due to physical weathering of crystalline sedimentary and metamorphic rocks. Weathering of Himalayan rocks is a major source for these clay minerals (Nath *et al.*, 2005). Kaolinite, on the other hand, is formed due to intense chemical weathering of bedrocks in warm and humid conditions (Nath *et al.*, 2005 and references therein). Alteration of terrestrial rocks in the sub-tropical and tropical belts, surrounding the Indian Ocean is a major source of kaolinite in this area. Smectite started to appear after 70cm from core top, with a broad peak range from 16.4-17.4Å (Fig 3b). Below 240cm upto the core bottom, smectites peaks are the most prominent among the clay minerals (Fig 3c). It has been reported in many earlier works that smectites in the CIOB are generated due to alterations of in situ submarine basalts in presence of biogenic silica (Kolla *et al.*, 1976; Rao and Nath, 1988; Valsangkar and Ambre, 2000). Quartz peak is ubiquitous in the entire core with a dominant peak at 3.34Å.

3.3. Radiolarian biostratigraphy:

The carbonate compensation depth (CCD) and the lysocline in the CIOB lie within 4400-4700m of water depth as per Banakar *et al.*, (1998). Whereas, Sabine *et al.*, (2002) have reported that calcite saturation depth is at around 3800m in the CIOB with a much shallower aragonite saturation depth (~1000m). Hence, no calcareous fossils are found in the present core as the core was located at a

water depth of 4935m, much below the CCD. Radiolarian index species are used instead to establish the biostratigraphy of the core. *Collosphaera (=buccinosphaera) invaginata*, *Collosphaeratuberosa*, *Collosphaeraorthoconus*, *Stylatractusuniversus*, *Anthocyrtiumnossicae*, *Amphirhopalumypsilon*, *Lamprocyrtisneoheteroporos*, *Lamprocyrtisheteroporos*, *Anthocyrtiumangulare*, *Theocorythiumvetulum*, and *Pterocaniumprismatium*, are searched for assigning the Quaternary datum levels as described in Johnson *et al.*, (1989) and illustrated in Gupta (1988). Identification of at least five Neogene Radiolarian zones (NR zones) is possible. Radiolarian biostratigraphy is summarized in Fig4. The top most and youngest zone, called *Collosphaera (=buccinosphaera) invaginata* zone (0-0.18Ma), is missing in the core. It could be either due to washing of the top few centimeters of sediment while coring or due to erosion of surface sediments by AABW (Banakar *et al.*, 1991). The upper 0-25cm section is represented by *Collosphaeratuberosa* zone (0.18-0.4Ma, NR-2), followed by *Stylatractusuniversus* zone (0.4-0.5Ma, NR-3) (Fig 2), *Amphirhopalumypsilon* zone (0.5-1.0Ma NR-4), *Anthocyrtiumangulare* zone (1.0-1.5Ma, NR-5), and the last one is *Pterocaniumprismatium* zone (1.5-2.0 Ma, NR-6). Species *Pterocaniumprismatium* is not found but *Theocorythiumvetulum* (Nigirini, 1971) is found, whereas *Lamprocyrtisneoheteroporos* and *L. heteroporos* are found in the *Amphirhopalumypsilon* zone, and they are considered as proxy representative of these two older zones.

The core section older than 125cm depth is having sparse radiolarian yield and devoid of any identifiable index fossil, whereas sections below 185cm is barren of radiolarian, but yielded unidentifiable micro-fish remains called the ichthyoliths. Based on the radiolarian biostratigraphy, the sedimentation rate of the core is determined and represented in Fig 5a. The top 0-50cm section of the core exhibited higher sedimentation rate of 0.18cm/kyr whereas lower 50-125cm exhibited lower sedimentation rate of 0.05cm/kyr. The age at this break corresponds to 500ka which marks Marine Isotope Stage 13 covering the Cromerian interglacial period between ~524 and 474kyr ago (Fig 5b). The core F200B from this area, exhibits sediment accumulation rates of 0.47 ± 0.15 cm/kyr from 0-40cm, 0.063 ± 0.007 cm/kyr from 41-55cm and 0.29 ± 0.06 cm/kyr from 55-76cm (obtained from $^{230}\text{Th}_{\text{ex}}$ activity vs depth) (Gupta, 1988; Sukumaran *et al.*, 1999). Two other cores from this area SK/226 and SK/657 exhibit a sediment accumulation rate of 0.2cm/kyr based on radiolarian stratigraphy, and in both of them the oldest sediments encountered are of 180ka age (Mudholkar *et al.*, 1993). Thus, the sedimentation rates found out in this study (0.05-0.18cm/kyr) falls within the range of the sediment accumulation rates of cores F200B, SK/226 and SK/657. The core depth and its geological ages are very similar to core F88B of Gupta (1988) which has an average

sedimentation rate of 0.08cm/kyr. (Borole, 1993) representing almost 2Ma record compressed in to ~125cm sediment and in good agreement with similar previous studies in the CIOB.

3.4. Major elements:

The concentrations of most of the major element oxides increased down core, with minimum concentrations at the surface and maximum at different depths (Table 1). A two-fold increase of detrital elements with depth, was observed by Pattan *et al.*, (2005) in a core AAS5/GC2 from a nearby location in siliceous zone of CIOB. Only SiO₂ and K₂O showed downward decrease with maximum concentrations at 5-10cm sections and sub-surface minima (Table 1). Among the major element oxides, TiO₂, Al₂O₃ and MgO are mostly derived from detrital materials. Fe₂O₃ and MnO are also primarily detrital in nature but can have other sources also. They can either precipitate hydrogenetically from the colloidal matters of the water column or undergo diagenetic dissolution at sub-surface depths due to reducing environment and migrate upwards through sediment pore waters in the upper oxic zones to be reprecipitated. CaO and Na₂O, on the other hand, are derived in the marine sediments mainly through weathering of alkaline rocks although CaO has an additional source in the form of calcium carbonate secreting marine biogenic community.

SiO₂, although is mainly detrital in nature, showed completely different trend than rest of the detrital element oxides. Besides continental (aluminosilicates, quartz, feldspars etc.) and local volcanic input (glass shards and other quartzo-feldspathic minerals), bulk silica also contains a significant amount of biogenic source (siliceous tests of micro-organisms), especially in the case of modern-day, oxic deep-sea sediments, formed at a greater depth than the local CCD. Thus "excess/biogenic" silica was calculated by using the formula adapted by Nath *et al.*, (1989), originally modified from Bostrom (1976):

$$\text{SiO}_2 (\text{ex/bio}) = \text{SiO}_2 \text{sample} - 3.38 (\text{Al}_2\text{O}_3 \text{sample}) \dots\dots\dots [1]$$

where, 3.38 is the SiO₂/Al₂O₃ ratio of average deep-sea clay (Turekian and Wedephol, 1961). The calculation is based on the fact that the SiO₂/Al₂O₃ ratio in terrigenous clay and deep-sea clay is more or less constant; averaging about 3.38 and the excess part is mainly derived from the radiolarian and diatomaceous oozes. In the present study, it can be seen that the maximum concentration of SiO₂_{excess} was obtained at 5-10cm section and gradually decreased down the core (Fig 6a), becoming negligible just above the transition zone (175-180cm section). The coarse fraction observation under microscope also gives a similar result of finding maximum radiolarian tests at 5-10cm depth interval.

The ratio between K_2O and Al_2O_3 can be used to determine the nature of weathering prevailed during sedimentation, i.e. whether physical weathering dominated at the time of deposition of the sediments or chemical weathering. Again, to understand the degree of alteration in these sediments due to diagenesis and other physico-chemical changes, the chemical index of alteration (CIA) has been calculated for each section of the studied core according to Nesbitt and Young (1982):

$$CIA = \{Al_2O_3 / (Al_2O_3 + CaO^* + Na_2O + K_2O)\} \times 100 \dots\dots\dots [2]$$

where, all the oxides are in molar proportion and CaO^* is the amount of CaO associated with the silicate fraction of the samples, excluding those combined with the carbonates and phosphates. Since, the present core lies at a water depth much below the CCD in this area, its CaO content is very low with a range of 0.84-1.52%. Hence, it can be safely mentioned here that whatever amount of CaO is present in this sediment core are mostly attached to the silicate fraction, rather than calcium carbonate. Therefore, the CIA actually reflects the degree of aluminum silicate minerals, especially feldspar weathered to clay minerals. In the present study, a distinct trend of increasing CIA values with depth has been found (Fig 6b) with minimum value at the core top. It was found out that the top 35cm of the core have a range of 40-50, below which it steadily increased and remained at an average range of 55-60 with a maximum value of 63 at 495-500cm depth (Fig 6b).

3.5 Trace and Rare Earth elements:

Among the trace metals, only Ba and Sr decreased down core, although their maximum and minimum concentrations are at different depth intervals (Table 2 and Fig 7). Co and V showed similar concentration profiles and both have maximum concentrations at the transition zone of 180-185cm and surface minima (Table 2 and Fig 7). Cu and Ni, on the other hand, have similar down core profile but different depth intervals of maximum and minimum concentrations (Table 2 and Fig 7). The concentrations of the Rare Earth Elements ($\sum REEs$) including yttrium, increased down core like most of the trace elements with a surface minimum (Table 2 and Fig 7). The maximum concentrations of most of the REEs are found at the bottom of the core, except Ce and Y. They have maximum concentrations at intermediate depths of 105-110cm and 365-370cm respectively (Table 2 and Fig 7). The concentrations of the trace elements of each sub-section are normalized by their respective Ti concentrations to obtain the amount which is not supported by the detrital fraction. Both Ti and Al can be used for this purpose as they are considered to be land derived mostly and hence, detrital in nature. However, Ti is used in this case as its concentration is not as high as Al. These normalized trace element distribution patterns differed markedly from the bulk element distribution patterns except for Sr and Ni (Fig 8). In Table 2 and Fig 7, it can be seen that most of the

trace elements had their minimum concentrations in the top 80cm of the sediment core with the exceptions of Ba, Sr and Ni only. Whereas, in case of Ti normalized trace elements (El/Ti), the minimum concentrations of most of them lie in a subsurface depth of 195-230cm, with the only exceptions of Ba, Co and V (Fig 8). Also, the maximum concentrations of most of the bulk elements lie at different subsurface depths, mostly in the lower part of the core (Table 2 and Fig 7). Whereas, El/Ti pattern shows that most of the elements have their maximum concentrations at the upper part of the core, above the transition zone, with the exceptions of Cu, Ni, Y and Σ REE (Fig 8). The PAAS normalized REE pattern, including Y, revealed middle REE (MREE) enrichment (Fig9), similar to the core SS/657 (Pattan and Banakar, 1997), which was described to be formed as a result of dissolution of micronodules at sub-surface depth. However, it may also occur due to post depositional alterations, for which preferential enrichment of MREE takes place (Shields and Stille, 2001). REEs are fractionated as follows: LREE into terrigenous, MREE into Mn-oxide and HREE into authigenic phosphate phases. These effects became more pronounced with increasing depth (Pattan *et al.*, 2005). Distinct negative Ce and positive Eu anomalies are observed throughout the length of the sediment core (Fig 9). Also, it is evident from Fig 9 that the upper sections of the core have less prominent negative Ce-anomaly compared to the lower sections. Negative Ce-anomaly might result from the presence of phillipsites, phosphorites and smectites, while positive anomaly results due to the presence of Fe-Mn oxyhydroxides (Pattan *et al.*, 2005) which is evident in this case.

4. Discussion:

4.1 Variation in clay mineralogy:

Down core clay mineralogy, showed that kaolinite and chlorite dominated the upper sections of the core with a lesser prominent peak of illite. The lower sections are dominated by smectite over other clay minerals. Among the clay minerals, only illite contains potassium in its framework structure from which potassium can be derived in the sediments (Yarincik *et al.*, 2000) other than potash feldspar (Zabel *et al.*, 2001). From Fig10, it can be seen that the K_2O/Al_2O_3 ratio of the sediments progressively increased in the younger sediments and became highest at the surface. In the older sediments, especially below the transition zone, K_2O/Al_2O_3 ratio is very less, about 0.13 on average. Also, the feldspar grains observed in the CF of the sediments are mainly plagioclase feldspars. Hence, in the older sediments, very low values of K_2O/Al_2O_3 ratio are mainly due to the dominance of smectites over illites in the clay fraction. With the gradual decrease of smectites in the younger sediments, K_2O/Al_2O_3 ratio also increased significantly in the upper part of the core. Thus, all these observations indicate that the area under study received heavy detrital input, prior to Quaternary, in

the form of volcanic materials mostly, for which smectites are more abundant than the other clay minerals. Intense chemical weathering of basalts under water produced sediments with higher CIA and lower K_2O/Al_2O_3 values due to the presence of more calcic plagioclase in these sediments. With time, the volcanic activity ceased gradually or there was a climatic shift which was reflected in the sedimentation pattern also. The sediment type changed from red clay to siliceous ooze with more physical weathering which increased the K_2O/Al_2O_3 ratio and decreased the CIA values of the younger sediments of the core.

4.2 Record of sedimentation:

The majority of coarse fraction of this core is made up of radiolarian tests which occur as radiolarian ooze or siliceous ooze. They are found as zooplanktons throughout the ocean. Other siliceous micro-organisms like diatoms and silicoflagellates were very less. No intact calcareous tests were observed due to the much higher water depth of the area which dissolved the calcareous fossils. Other than that, some unidentifiable micro-fish remains, called the ichthyoliths, are observed. Below 180-185cm depth, the core is completely devoid of radiolarian tests or any kind of biological remnants. This absence is not just due to the dissolution of radiolarian tests due to compaction within the core, but mainly due to the change in lithofacies from siliceous ooze to pelagic clay. The mineralogy and other physical parameters of the sediment also changes markedly as are mentioned in the previous sections. This is a significant finding of this study as such detailed lithological observations were not performed on a sediment core from this area, having a continuous length of 5.4m.

The sedimentation rate, calculated from the radiolarian age shows, that there was a sudden change from 0.05 to 0.18cm/kyr which occurred at around 500kyr. This age corresponds with MIS 13 marking the Cromerian Interglacial period in Britain which is well recorded from $\delta^{18}O$ values. The details of the dating and stacking technique are well explained in Lisiecki and Raymo (2005) along with standard error for each reading, from which the $\delta^{18}O$ values are taken. The Cromerian Stage or the Cromerian warm period is a stage consisting of multiple glacial and interglacial periods in the Middle Pleistocene epoch. The name arrives from the town of Cromer in England where interglacial deposits of this stage was first discovered from coastal cliff. The record of MIS 13 has been also shown in a core from Indian Ocean, off shore Australia, where very good resemblance in trends are presented between MIS stages and $\delta^{18}O$ values of foraminifera based on which the age of the core is determined (Spooner et al, 2011; Stuut *et al*, 2014). This core has recorded warmer interglacial and drier glacial periods due to 3-4° northward migration of the Indonesian Through flow Water/South Indian Central Water frontalsystem which brought warmer water from the Indo Pacific Warm Pool

in Central Indian Ocean (Spooner *et al.*, 2011). Moreover, a major climatic shift happened immediately after this period, called the Mid-Brunhes shift (MBS) at around 430kyr ago which marks the transition from MIS 12 to MIS 11. Increased amplitude of glacial-interglacial cycles leading to higher sea-surface temperature (SST) globally started much before MBS but peaked during 430kyr as is recorded from different basins all around the world from the study of radiolarian fossils (Jansen *et al.*, 1986). Also, it was observed that the polar fronts in the North Pacific, South Atlantic, South East Indian Oceans and the interglacial subtropical fronts in the Canary Basin were situated more towards the north during the early Brunhes, which shifted southwards after this climatic change (Jansen *et al.*, 1986). The effect of this event was also observed at a core further south-west from ours (Nath *et al.*, 2013). Although in our sediment core, no significant physico-chemical change was observed corresponding to MBS, nevertheless the marked increase in bioproductivity leading to increased sedimentation rate at around 500kyr in the studied core can be a cumulative effect of these two consecutive, prominent warming events. Thus, it will be the first report of these kinds of events recorded in an Indian Ocean sediment core. Further study with robust dating technique is planned in future which will bring new insights in this field.

4.3 Major elements:

Most of the major element oxides decreased down core with the exception of SiO_2 and K_2O only, indicating more detrital character of the lower part of the core, than the upper part. A major part of silica was mainly derived from the siliceous tests of radiolaria which constitute >90% of the CF population in the top 125cm section of the core. Other than that, dissolution of glass shards and other volcanogenic materials like pumice, palagonite, zeolite crystals also contributed to the excess silica content. The maximum concentration of $\text{SiO}_{2\text{excess}}$ was obtained at 5-10cm section which matches very well with the microscopic observation of CF components as the highest number of radiolarian tests was observed in the same section of the core. The CIA values of fresh basalts range between 30-45, granites and granodiorites 45-55 whereas, average shales range between 70-75 due to the presence of clay minerals like muscovite (75), illite, montmorillonite (75-85), kaolinite and chlorite (close to 100) (Nesbitt and Young, 1982). Hence, a range of 55-60, in the present study, seems to be an intermediate between a basaltic precursor and weathered clay minerals comprising more of illite, muscovites towards the top of the core and kaolinite, chlorite and mainly smectites near the bottom. All these findings further reconfirm the fact that a significant climatic change occurred in this area which not only affected the sedimentation pattern but its character also.

4.4 Trace elements and Rare Earth elements:

Ti normalized trace elements represent the part of trace elements which are of non-detrital origin, that is they are either precipitated authigenically or biogenically in the system or are enriched via diagenetic processes in the sediment column. The down core profiles of El/Ti ratios of most of the trace elements exhibit a similar trend except Ba and Sr. From core bottom towards the top, the values continued to decrease at first. Within 180-320cm of the core, most of the El/Ti ratios exhibited lowest values, reaching minimum at the transition zone (180-185cm). Above the transition zone, the ratios increased steadily towards the core top. This trend is typically observed in almost all deep-sea cores (Pattan and Banakar, 1997; Pattan *et al.*, 2005). The micronodules of the CF are a major source of redox sensitive elements like Cu, Ni, Co and V along with REEs in these sediments, which can be seen from the good positive correlations among these elements as well (Table 4a and 4b). The dissolution of micronodules in the intermediate depth releases these elements into the sediment pore water which migrate upward and get incorporated into the Fe-Mn oxyhydroxide phases due to the prevailing oxic condition. That is why, a sub-surface low concentration of Cu, Ni, Co, V and REEs was observed in this core between 180-325cm sections of the core. This is also the reason for getting PAAS normalized MREE enriched pattern in this core which is a result of post depositional alterations as reported by Shields and Stille (2001) at sub-surface depth. Sr/Ti, on the other hand, differed from this trend and increased steadily from core bottom towards top, with maximum concentration at 30-35cm depth. Ba/Ti also showed a similar trend like Sr/Ti, with maximum concentration at 30-35cm depth, although there is another peak at 245-250cm depth. Infact, between 205-300cm of the core, Ba/Ti shows an increase in concentration, unlike most of the other trace elements. Ba is known to be associated with organic matter and gets mobilized under reduced-suboxic condition (Dymond *et al.*, 1992). Formation of authigenic barite in oceanic particles is considered to be a consequence of uptake by organic carbon rather than secretion of barite by any particular organism (Dymond *et al.*, 1992). Hence, this could be the reason behind increased Ba/Ti ratio in intermediate depth, corresponding to decreased El/Ti ratios (except Sr). Their similar behavior is also observed from Table 4a and 4b where they are well correlated to each other both before and after Ti normalization. On the other hand, Sr is mostly associated with bio-productivity as it can replace Ca and hence Sr/Ti ratio showed an overall increasing trend from core bottom towards top, much like SiO₂.

REEs are generally incompatible in nature, trivalent and behaves coherently more or less. However, Ce and Eu have more than one valence states, for which they get relatively enriched or depleted than other REEs. Ce is sensitive under oceanic redox conditions and becomes 4+ when oxidized. Hence, highly oxic deposits like ferromanganese nodules exhibit positive Ce-anomaly and

the surrounding water or sediments from where it is deposited, show negative anomalies (Banakaret *et al.*, 1998). Goldberg *et al.*, (1963), Piper (1974a & b), Tlig and Steinberg (1982) reported that, negative Ce-anomaly, in marine sediments, might also result from the presence of zeolites, phosphorites and smectites. Thus, this could be the reason of negative Ce-anomaly in the sediments of the core AAS-38/4, as abundant smectite was found in this core with occasional presence of zeolite. In fact, Ce does not show strong positive correlation with other redox sensitive trace elements as well as Σ REEs except Sr (Table 4a). However, after Ti normalization Ce does show positive correlation with other trace elements except Cu, Ni and Y (Table 4b). Again, like Ce, Eu also has two valence states, Eu^{2+} in reducing condition which is very similar to Ca^{2+} due to their similar charge and ionic radius. Hence, it can easily replace Ca during magmatic processes in minerals like plagioclase. However, redox condition of Eu does not normally take place with in the ocean, unlike Ce. Hence, positive Eu-anomaly in this sediment core, was observed due to the presence of volcanic materials like plagioclase and palagonite crystals.

5. Conclusions:

A distinct change in depositional environment occurred in the Central Indian Ocean Basin which affected the sedimentation pattern in the core AAS-38/4 from dominantly red clay to siliceous ooze sediment. The pre-Quaternary red clay sediments of this core, received more detrital inputs in the form of volcanogenic materials, comprising mostly of glass shards, pumice, palagonite and occasional zeolite crystals. Intense chemical weathering prevailed in this area for which smectite dominated the clay fraction as a result of sub-aqueous alteration of basalts. From Quaternary onwards, the lithofacies changed to siliceous ooze dominated by radiolarian tests and physical weathering became more prominent over chemical weathering. This resulted in the disappearance of smectites from the clay fraction and kaolinite, chlorite and illite as the major clay minerals in the younger sediments. Based on radiolarian stratigraphy an age of 2.0 Ma was determined up to 125 cm depth from the core top. After the initial transition of the lithofacies, the sedimentation rate was low, about 0.05 cm/kyr within the top 50-125 cm depth of the core, above which it increased to 0.18 cm/kyr due to higher bio-productivity. This change in sedimentation pattern occurred at around 500 kyr which coincides with the Marine Isotope Stage 13 or the Cromerian interglacial period in the Middle Pleistocene epoch which marks a distinct shift in climatic regime from a colder to a warmer episode. Also, MIS 13 is shortly followed up by the more global warming event of Mid-Brunhes shift which marks the increase of amplitude of glacial-interglacial cycles with a corresponding shift of subtropical fronts. Thus, the change in lithofacies, decrease of detrital components with a

corresponding increase in bio-productivity and sedimentation rate could be a cumulative effect of these two significant warming events.

Acknowledgement:

The authors are thankful to the Director, CSIR-NIO, Goa for permitting to carry out this work. S. Sensarma gratefully acknowledges the support of CSIR Senior Research Fellowship, India. This work is a part of the Council of Scientific and Industrial Research (CSIR) supported by GAP-2175 and bears NIO contribution number XXXX.

References:

- Banakar, V.K., Gupta, S.M., Padmavathi, V.K., 1991. Abyssal sediment erosion in the Central Indian Basin: Evidence from radiochemical and radiolarian studies. *Mar. Geol.*, 96, 167-173.
- Banakar, V.K., Parthiban, G., Pattan, J.N., Jauhari, P., 1998. Chemistry of surface sediment along a north-south transect across the equator in the Central Indian Basin: an assessment of biogenic and detrital influences on elemental burial on the seafloor. *Chem. Geol.*, 147, 217-232.
- Borole, D.V., 1993. Late Pleistocene sedimentation: a case study of the Central Indian Basin, Indian Ocean. *Deep Sea Res.Pt. I*, 40(4), 761-775.
- Bostrom, K., 1976. Particulate and dissolved matter as sources for pelagic sediments. *Stockholm Contrib. Geol.*,30, 15-79.
- Brady, M., Bowie, C., 2017. Discontinuity surfaces and microfacies in a storm-dominated shallow Epeiric Sea, Devonian Cedar Valley Group, Iowa. *The Depo. Rec.*, 3(2),136–160.
- Christ, N., Immenhauser, A., Amour, F., Mutti, M., Tomás, S., Agar, S.M., Alway, R. and Kabiri, L., 2012. Characterization and interpretation of discontinuity surfaces in a Jurassic ramp setting (High Atlas, Morocco). *Sedimentology*, 59, 249-290. <https://doi.org/10.1111/j.1365-3091.2011.01251.x>.
- Dymond, J., Suess, E., Lyle, M., 1992. Barium in deep-sea sediment: A geochemical proxy for paleoproductivity. *Paleoceanography*, 7 (2), 163-181.
- Folk, R.L.,1968. *Petrology of Sedimentary Rocks*. Hemphill's, Austin, Texas pp:170.
- Gupta, S.M., 1988. Radiolarian zonation and volcanic ash layers in two Quaternary sediment cores from the Central Indian Ocean Basin. *J.Palaeontol. Soc. Ind.*, 33, 59-71.
- Hillgärtner, H., 1998. Discontinuity surfaces on a shallow-marine carbonate platform (Berriasian, Valanginian, France and Switzerland). *J. Sediment. Res.*, 68, 1093–1108.
- Iyer, S.D., Shyam Prasad, M., Gupta, S.M., Charan, S.N., 1997. Evidence for recent hydrothermal activity in the Central Indian Basin. *Deep Sea Res. Pt. I*, 44 (7), 1167-1184.
- Iyer, S.D., Fernandes, G.Q., Mahender, K., 2012. Coarse fraction components in a red-clay sediment core, Central Indian Ocean Basin: their occurrence and significance. *J. Ind. Assoc.Sedimentol.*, 31(1-2), 123-135.

- Jansen, J.H.F., Kuijpers, A., Troelstra, S.R., 1986. A Mid-Brunhes climatic event: Long-term changes in global atmosphere and ocean circulation. *Science*, 232, 619-622.
- Johnson, D.A., Schneider, D.A., Nigrini, C.A., Caulet, J.P., Kent, D.V., 1989. Pliocene-Pleistocene radiolarian events and magnetostratigraphic calibrations for the tropical Indian Ocean. *Mar. Micropal.*, 14(1-3), 33–66.
- Kolla, V., Sullivan, L., Streeter, S.S., Langseth, M.G., 1976. Spreading of Antarctic bottom water and its effects on the floor of the Indian Ocean inferred from bottom-water potential temperature, turbidity and sea floor photography. *Mar. Geol.*, 21, 171-189.
- Lisiecki, L.E., Raymo, M.E., 2005. A Pliocene-Pleistocene stack of 57 globally distributed benthic $\delta^{18}\text{O}$ records. *Paleoceanography*, 20, PA1003, 1-17. doi:10.1029/2004PA001071.
- Mudholkar, A.V., Pattan, J.N., Parthiban, G., 1993. Geochemistry of deep-sea sediment cores from the Central Indian Ocean Basin. *Ind. J. Mar. Sc.*, 22, 241-246.
- Nath, B.N., Rao, V.P., Becker, K.P., 1989. Geochemical evidence of terrigenous influence in deep-sea sediments upto 8°S in the Central Indian Basin. *Mar. Geol.*, 87, 301-313.
- Nath, B.N., Gupta, S.M., Mislankara, P.G., Rao, B.R., Parthiban, G., Roelandts, I., Patil, S.K., 2005. Evidence of Himalayan erosional event at ~0.5Ma from a sediment core from the equatorial Indian Ocean in the vicinity of ODP Leg 116 sites. *Deep Sea Res. Pt. II*, 52, 2061–2077.
- Nath, B.N., Sijinkumar, A.V., Borole, D.V., Gupta, S.M., Mergulhao, L.P., Pereira, M.B.L.M., Ramaswamy, V., Guptha, M.V.S., Possnert, G., Aldahan, A., Khadge, N.H., Sharma, R., 2013. Record of carbonate preservation and the Mid-Brunhes climatic shift from a seamount top with low sedimentation rates in the Central Indian Basin. *Boreas*, 42, 762–778.
- Nesbitt, H.W., Young, G.M., 1982. Early Proterozoic climates and plate motions inferred from major element chemistry of lutites. *Nature*, 299, 715-717.
- Nigrini, C.A., 1971. Radiolarian zones in the Quaternary of the Equatorial Pacific Ocean. In: Funnel, B.M., Riedel, W.R. (Eds.), *The Micropaleontology of Oceans*. Cam. Univ. Press, pp.443-461.
- Pattan, J.N., Banakar, V.K., 1997. Diagenetic remobilization of Rare Earth elements in a sediment core from the Central Indian Basin. *Ind. J. Mar. Sc.*, 26, 341-344.
- Pattan, J.N., Pearce, N.J.G., Mislankar, P.G., 2005. Constraints in using Cerium-anomaly of bulk sediments as an indicator of paleo bottom water redox environment: A case study from the Central Indian Ocean Basin. *Chem. Geol.*, 221, 260–278.
- Pereira, M.B.L.M., Nath, B.N., Borole, D.V., Gupta, S.M., 2006. Nature, source and composition of volcanic ash in sediments from a fracture zone trace of Rodriguez Triple Junction in the Central Indian Basin. *Mar. Geol.*, 229, 79–90.
- Rao, V.P., Nath, B.N., 1988. Nature, Distribution and Origin of Clay Minerals in Grain Size Fractions of Sediments from Manganese Nodule Field, Central Indian Ocean Basin. *Ind. J. Mar. Sc.*, 17, 202-207.
- Ray, D., Kota, D., Das, P., SuryaPrakash, L., Khedekar, V.D., Paropkari, A.L., Mudholkar, A.V., 2014. Microtexture and distribution of minerals in hydrothermal Barite-Silica chimney from the

Franklin seamount, SW Pacific: Constraints on mode of formation. *Ac. Geol. Sin. Eng.*, 88(1), 213-225.

Spooner, M.I., Deckker, P.D., Barrows, T.T., Fifield, L.K., 2011. The behaviour of the Leeuwin Current offshore NW Australia during the last fiveglacial-interglacial cycles. *Glob. Planet. Change*, 75, 119-132.

Stuut, J.W., Temmesfeld, F., Dekker, P.D., 2014. A 550ka record of aeolian activity near North West Cape, Australia:inferences from grain-size distributions and bulk chemistry of SEIndian Ocean deep-sea sediments. *Quat. Sci. Rev.*, 83, 83-94.

Sukumaran, N.P., Banerjee, R., Borole, D.V., Gupta, S.M., 1999. Some aspects of volcanic ash layers in the Central Indian Basin. *Geo-Mar. Lett.*, 18, 203-208.

Turekian, K.K., Wedepohl, K.H., 1961. Distribution of the Elements in some major units of the Earth's crust. *Geol. Soc. Am. Bull.*, 72, 175-192.

Valsangkar, A.B., Ambre, N.V.,2000. Distribution of Grain Size and Clay Minerals in Sediments from the INDEX Area, Central Indian Basin. *Mar. Georesources. Geotechnol.*, 18, 189-199.

Yarincik, K.M., Murray, R.W., Peterson, L.C., 2000. Climatically sensitive eolian and hemipelagic deposition in the Cariaco Basin, Venezuela, over the past 578,000 years: Results from Al/Ti and K/Al. *Paleoceanography*, 15, 210–228.

Zabel, M., Schneider, R.R., Wagner, T., Adegbe, A.T., de Vries, U., Kolonic, S., 2001. Late Quaternary Climate Changes in Central Africa as Inferred from Terrigenous Input to the Niger Fan. *Quat. Res.*, 56, 207–217.

List of Tables:

Table 1: Major element oxide concentrations of each sub-sections of the sediment core AAS-38/4in weight%.

Sr. No.	Depth (cm)	SiO ₂	Al ₂ O ₃	TiO ₂	Fe ₂ O ₃	MnO	MgO	CaO	Na ₂ O	K ₂ O
1	0-5	42.72	7.11	0.26	3.37	0.61	1.95	0.98	7.53	1.68
2	5-10	51.86	9.35	0.26	3.54	0.81	1.97	1.27	7.10	2.12
3	10-15	51.42	9.79	0.30	4.10	1.01	2.13	1.19	7.14	1.97
4	15-20	49.51	9.89	0.30	4.33	1.06	2.16	0.90	6.50	1.88
5	20-25	48.68	9.87	0.31	4.31	1.00	2.14	1.32	6.80	1.81
6	25-30	49.25	10.58	0.32	4.66	1.02	2.37	0.84	7.40	1.92
7	30-35	48.20	10.57	0.32	4.61	1.04	2.32	1.26	7.49	1.90
8	35-40	46.46	10.79	0.33	4.77	1.04	2.35	1.35	6.59	1.94
9	40-45	47.75	11.46	0.37	5.15	1.05	2.47	1.27	6.91	2.00
10	45-50	47.94	11.68	0.39	5.30	1.07	2.52	1.07	6.61	2.03
11	50-55	47.36	11.68	0.39	5.30	1.08	2.46	0.95	6.79	2.01
12	55-60	46.88	11.77	0.41	5.40	1.07	2.50	0.95	6.56	2.03
13	60-65	47.32	11.82	0.41	5.38	1.09	2.56	0.96	6.50	2.03
14	65-70	47.55	11.98	0.42	5.42	1.08	2.66	1.19	6.88	2.02
15	70-75	46.71	12.02	0.41	5.44	1.03	2.64	1.01	6.92	2.02
16	75-80	46.41	12.21	0.42	5.50	1.06	2.66	1.24	7.01	2.01
17	80-85	45.42	11.94	0.42	5.48	1.04	2.67	1.08	6.01	1.99
18	85-90	45.51	12.05	0.42	5.49	1.05	2.69	1.08	6.43	2.01
19	90-95	46.85	12.44	0.44	5.65	1.11	2.80	1.00	6.84	2.04
20	95-100	44.95	12.28	0.44	5.67	1.10	2.85	1.13	6.29	2.02
21	100-105	45.76	12.41	0.43	5.65	1.14	2.89	1.11	6.49	2.01
22	105-110	45.33	12.39	0.43	5.65	1.11	2.91	1.18	6.93	1.99
23	110-115	45.02	12.18	0.41	5.55	1.11	2.95	1.15	6.96	1.97
24	115-120	45.02	12.27	0.41	5.68	1.09	3.00	0.92	6.51	2.00
25	120-125	44.36	12.15	0.42	5.63	1.06	2.98	1.05	6.53	1.94
26	125-130	45.12	12.47	0.42	5.66	1.11	3.12	1.52	7.10	1.95
27	130-135	44.40	12.73	0.45	6.44	1.15	3.17	1.04	6.31	1.97
28	135-140	43.86	12.64	0.44	6.01	1.14	3.18	0.97	6.36	1.95
29	140-145	42.45	12.04	0.43	5.89	1.09	3.17	1.06	6.18	1.88
30	145-150	43.90	12.56	0.42	5.66	1.16	3.16	1.22	7.18	1.91
31	150-155	44.19	12.67	0.42	5.72	1.14	3.11	1.09	6.97	1.93
32	155-160	44.32	12.49	0.42	5.61	1.16	3.09	1.01	7.17	1.89
33	160-165	43.75	12.35	0.42	5.60	1.15	3.15	1.11	7.43	1.86
34	165-170	44.13	12.57	0.43	5.70	1.16	3.21	1.28	7.44	1.86
35	170-175	43.58	12.43	0.43	5.67	1.12	3.13	1.05	8.25	1.89
36	175-180	44.39	13.03	0.45	5.93	1.15	3.30	1.03	7.15	1.90
37	180-185	42.89	13.30	0.45	5.99	1.13	3.40	1.13	7.31	1.82
38	185-190	42.85	13.53	0.47	6.22	1.15	3.45	0.99	7.35	1.83
39	190-195	42.69	14.13	0.51	6.63	1.18	3.67	1.02	6.43	1.82

Table 1 contd/...

Sr. No.	Depth (cm)	SiO ₂	Al ₂ O ₃	TiO ₂	Fe ₂ O ₃	MnO	MgO	CaO	Na ₂ O	K ₂ O
40	195-200	41.72	13.91	0.50	6.38	1.17	3.73	1.15	7.17	1.77
41	200-205	42.10	14.14	0.50	6.53	1.16	3.62	0.98	6.83	1.78
42	205-210	41.83	14.13	0.50	6.42	1.15	3.68	1.01	6.88	1.76
43	210-215	41.92	14.02	0.49	6.41	1.20	3.67	1.11	6.71	1.76
44	215-220	42.50	14.16	0.50	6.48	1.13	3.64	1.06	6.55	1.78
45	220-225	41.72	13.85	0.48	6.25	1.16	3.66	1.07	6.55	1.72
46	225-230	41.53	13.89	0.47	6.15	1.20	3.79	1.05	6.83	1.69
47	230-235	41.54	13.87	0.47	6.18	1.20	3.75	1.05	6.80	1.69
48	235-240	42.26	13.98	0.46	6.22	1.16	3.75	1.04	7.13	1.71
49	240-245	41.82	13.95	0.45	6.12	1.14	3.69	1.15	7.49	1.69
50	245-250	41.60	13.94	0.45	6.10	1.13	3.81	1.05	6.72	1.69
51	250-255	42.01	14.23	0.44	6.05	1.13	3.87	1.14	7.02	1.71
52	255-260	42.47	13.97	0.44	6.10	1.13	3.83	1.07	7.05	1.72
53	260-265	40.28	13.29	0.42	5.76	1.08	3.79	1.24	7.76	1.66
54	265-270	42.34	14.01	0.44	6.09	1.26	3.84	1.07	7.00	1.72
55	270-275	42.53	14.02	0.45	6.15	1.16	3.85	1.18	6.88	1.75
56	275-280	42.63	14.12	0.46	6.39	0.77	3.77	1.01	6.69	1.79
57	280-285	42.26	14.08	0.47	6.25	1.27	3.89	1.07	6.99	1.79
58	285-290	42.83	14.24	0.47	6.38	1.21	3.82	1.03	6.77	1.83
59	290-295	41.91	14.09	0.47	6.26	1.15	3.77	1.11	6.46	1.81
60	295-300	42.40	14.10	0.47	6.23	1.13	3.77	1.08	6.94	1.87
61	300-305	42.85	14.22	0.47	6.26	1.13	3.85	1.27	6.76	1.89
62	305-310	43.26	14.52	0.48	6.32	1.18	3.75	1.01	6.45	1.94
63	310-315	40.91	13.73	0.45	5.85	1.06	3.55	1.07	9.34	1.82
64	315-320	42.65	14.46	0.48	6.14	1.13	3.89	1.01	6.96	1.88
65	320-325	42.01	14.24	0.47	6.02	1.07	3.82	1.19	6.98	1.81
66	325-330	42.60	14.45	0.47	6.11	1.07	3.86	1.02	7.01	1.83
67	330-335	42.29	14.37	0.46	6.04	1.05	3.90	1.00	7.36	1.82
68	335-340	41.66	14.15	0.46	5.92	1.08	3.90	1.02	7.27	1.77
69	340-345	42.37	14.33	0.46	5.94	1.11	4.06	1.05	7.36	1.80
70	345-350	42.18	14.22	0.44	5.78	1.08	4.05	1.10	7.20	1.77
71	350-355	41.07	13.73	0.42	5.53	1.03	3.93	1.22	6.94	1.72
72	355-360	42.50	14.03	0.43	5.73	1.06	3.96	1.22	6.78	1.80
73	360-365	42.33	13.99	0.43	5.73	1.04	3.95	1.26	6.82	1.78
74	365-370	43.30	14.38	0.45	5.93	1.10	4.09	1.11	7.12	1.83
75	370-375	43.13	14.25	0.43	5.81	1.02	4.18	1.14	7.11	1.81
76	375-380	43.03	14.14	0.41	5.67	1.07	4.05	1.20	7.03	1.80
77	380-385	43.24	14.13	0.42	5.76	1.08	4.11	1.09	6.92	1.84
78	385-390	42.93	13.99	0.42	5.74	1.11	4.04	1.11	7.10	1.81
79	390-395	42.87	14.04	0.42	5.82	1.14	4.07	1.16	6.88	1.83
80	395-400	42.25	13.84	0.43	5.91	1.12	4.00	1.08	6.81	1.75
81	400-405	42.31	13.96	0.45	6.10	1.11	4.01	1.18	7.06	1.75

Table 1 contd/...

Sr. No.	Depth (cm)	SiO ₂	Al ₂ O ₃	TiO ₂	Fe ₂ O ₃	MnO	MgO	CaO	Na ₂ O	K ₂ O
82	410-415	41.28	13.76	0.47	6.06	1.12	3.96	1.30	7.15	1.71
83	415-420	41.44	13.83	0.46	6.02	1.15	3.98	1.21	7.20	1.72
84	420-425	41.86	13.96	0.46	5.98	1.13	3.93	1.24	7.23	1.73
85	425-430	41.69	13.85	0.44	5.91	1.14	3.92	1.19	7.26	1.72
86	430-435	40.93	13.46	0.43	5.67	1.16	4.11	1.22	7.27	1.63
87	435-440	40.31	13.21	0.43	5.65	1.10	3.90	1.16	6.78	1.62
88	440-445	41.17	13.65	0.45	5.81	1.11	4.00	1.17	7.79	1.71
89	445-450	40.92	13.57	0.45	5.85	1.11	3.92	1.08	6.96	1.68
90	450-455	41.29	13.90	0.47	6.01	1.12	4.01	1.11	7.14	1.71
91	455-460	41.29	13.94	0.47	5.95	1.08	4.02	1.20	7.22	1.65
92	460-465	40.96	13.73	0.43	5.79	1.10	4.03	1.08	7.09	1.63
93	465-470	41.74	13.84	0.43	5.78	1.11	4.06	1.10	6.96	1.64
94	470-475	40.73	13.53	0.43	5.64	1.08	3.95	1.14	7.28	1.66
95	475-480	40.05	13.25	0.42	5.61	1.08	3.84	1.12	7.52	1.64
96	480-485	41.25	13.78	0.45	5.95	1.12	3.86	1.00	7.06	1.71
97	485-490	42.28	14.21	0.48	6.30	1.16	3.88	0.94	6.91	1.77
98	490-495	41.50	14.04	0.49	6.42	1.19	3.99	0.99	6.58	1.79
99	495-500	42.77	14.41	0.48	6.43	1.19	3.77	0.94	5.70	1.81
100	500-505	41.45	13.92	0.46	6.15	1.17	3.76	1.02	6.61	1.76
101	505-510	41.77	14.00	0.46	6.15	1.22	3.85	1.05	6.53	1.77
102	510-515	41.86	13.94	0.45	6.14	1.23	3.90	1.06	6.79	1.76
103	515-520	41.83	13.95	0.46	6.14	1.25	3.94	1.04	6.45	1.75
104	520-525	41.59	13.66	0.44	6.01	1.27	3.88	1.09	6.22	1.72
105	525-530	43.14	14.04	0.44	6.13	1.32	4.09	1.15	5.69	1.78
106	530-535	42.56	13.81	0.44	6.13	1.34	4.13	1.26	6.66	1.74
107	535-540	41.89	13.56	0.42	6.06	1.29	4.05	1.15	6.67	1.75
Average		43.37	13.19	0.43	5.80	1.11	3.49	1.10	6.93	1.82
Max		51.86	14.52	0.51	6.63	1.34	4.18	1.52	9.34	2.12
Min		40.05	7.11	0.26	3.37	0.61	1.95	0.84	5.69	1.62

Table 2: Trace element concentrations of each sub-sections of the sediment core AAS-38/4 in mg/kg.

Sr. No.	Depth (cm)	Ba	Sr	Co	V	Cu	Ni	ΣREE	Ce	Y
1	0-5	817.9	148.8	54.50	48.65	181.6	105.0	199.12	74.28	54.39
2	5-10	917.7	158.4	53.25	53.06	180.3	76.55	219.92	80.93	59.72
3	10-15	1165	181.4	68.62	62.23	198.6	106.5	261.28	91.99	73.67
4	15-20	1317	183.2	70.61	60.17	216.7	118.1	263.14	91.13	75.78
5	20-25	1425	195.7	71.58	59.05	202.6	113.7	265.82	92.28	77.03
6	25-30	1403	172.5	58.92	60.52	190.0	159.6	229.78	79.16	65.66
7	30-35	1740	216.0	75.71	72.63	208.9	112.7	288.51	99.52	84.40
8	35-40	1722	208.8	76.16	73.16	214.2	117.0	291.95	98.78	87.26
9	40-45	1722	208.8	88.14	84.53	226.6	129.4	291.95	98.78	87.26
10	45-50	1589	211.7	81.28	87.65	228.6	167.7	303.77	109.5	81.64
11	50-55	1463	182.0	76.42	78.38	192.3	105.1	270.26	94.91	74.80
12	55-60	1332	180.1	79.88	74.68	209.6	120.0	293.49	102.5	85.20
13	60-65	1263	171.8	78.83	78.54	206.3	121.7	290.61	100.1	83.87
14	65-70	1159	181.9	76.69	75.99	222.0	166.7	297.74	102.6	87.28
15	70-75	1380	190.8	82.96	82.23	215.7	121.3	330.22	109.1	101.0
16	75-80	1111	169.6	70.36	68.70	178.5	90.99	279.94	92.08	84.32
17	80-85	1155	163.5	73.66	79.76	207.7	125.3	292.17	99.08	85.25
18	85-90	1159	170.9	79.45	84.30	229.4	143.1	320.61	105.4	94.61
19	90-95	971.6	170.9	80.21	92.98	257.9	203.0	325.80	106.9	95.53
20	95-100	1089	160.5	79.06	83.12	232.0	150.2	303.18	104.8	84.65
21	100-105	1250	168.3	79.12	82.71	235.7	157.8	310.09	106.5	86.73
22	105-110	1305	182.5	85.32	86.67	255.8	177.0	332.57	115.4	91.93
23	110-115	1682	210.5	94.82	95.08	253.3	119.9	351.29	96.02	109.7
24	115-120	1302	168.8	84.43	81.85	239.5	113.8	319.43	96.05	99.71
25	120-125	1318	179.1	83.82	85.38	233.7	104.8	352.01	109.5	107.4
26	125-130	1240	188.3	92.37	90.09	250.7	116.5	356.22	102.1	112.5
27	130-135	1171	165.3	94.50	91.03	257.5	130.0	348.06	105.9	108.5
28	135-140	1270	171.4	92.30	91.87	242.9	122.8	340.66	100.0	107.0
29	140-145	1325	168.5	87.88	80.93	234.5	116.7	345.44	109.8	105.9
30	145-150	1463	178.3	92.59	91.79	242.1	124.0	341.43	106.2	106.9
31	150-155	1340	175.4	94.05	89.59	240.9	121.2	348.52	111.5	105.3
32	155-160	1358	174.1	90.14	84.74	230.9	118.7	340.54	109.8	104.3
33	160-165	950.9	132.6	72.31	68.33	186.5	91.62	273.79	89.16	82.24
34	165-170	1137	167.1	87.36	85.23	224.3	108.6	321.03	109.3	91.09
35	170-175	1172	175.0	92.73	100.4	241.6	121.7	345.67	104.9	103.2
36	175-180	1103	167.4	96.15	92.99	238.6	113.7	337.11	103.2	100.9
37	180-185	1331	196.5	103.0	109.8	267.7	111.8	333.93	81.58	107.4
38	185-190	1259	178.8	97.79	105.8	252.1	103.2	326.67	104.9	92.91
39	190-195	1029	137.6	83.03	89.21	229.8	86.35	275.07	100.2	72.98
40	195-200	917	133.5	72.49	78.46	200.3	73.39	261.88	92.08	70.98

Table 2 contd/...

Sr. No.	Depth (cm)	Ba	Sr	Co	V	Cu	Ni	∑REE	Ce	Y
41	200-205	1134	150.3	82.97	93.02	229.9	90.10	304.07	107.1	83.93
42	205-210	1506	128.7	73.23	80.82	269.1	198.3	229.41	82.76	60.74
43	210-215	1781	155.3	83.92	90.07	295.1	234.1	283.21	77.17	86.67
44	215-220	1610	149.7	85.07	89.79	292.9	214.1	283.72	76.57	89.12
45	220-225	1776	160.3	86.90	89.44	324.3	229.1	312.28	84.18	96.33
46	225-230	1894	116.7	89.91	72.83	340.0	246.2	265.34	85.13	71.47
47	230-235	1308	123.7	68.98	74.62	260.7	199.1	253.81	83.98	74.70
48	235-240	1963	161.9	77.37	82.09	296.5	226.4	304.98	93.58	93.33
49	240-245	1660	145.3	70.86	75.49	269.6	193.3	286.90	90.00	86.43
50	245-250	2431	175.4	83.45	88.16	318.2	210.8	329.39	80.39	110.9
51	250-255	1959	155.5	72.76	77.31	273.1	186.3	310.38	95.03	97.12
52	255-260	2057	169.8	82.19	85.65	309.9	210.1	331.09	90.88	112.0
53	260-265	1516	135.8	68.68	71.56	257.3	176.6	279.30	84.84	89.84
54	265-270	1693	153.7	79.36	84.14	314.2	242.0	312.22	92.14	97.90
55	270-275	1680	146.1	71.09	78.46	300.3	233.2	317.02	93.39	101.0
56	275-280	960.4	117.0	73.42	74.80	274.6	150.0	272.76	83.87	84.74
57	280-285	1518	158.9	83.71	94.42	363.8	273.0	315.90	80.44	102.4
58	285-290	1584	160.3	86.26	94.78	359.7	244.2	324.49	83.22	105.6
59	290-295	1733	152.8	78.49	86.02	314.2	209.1	304.34	76.02	99.87
60	295-300	1542	144.4	86.57	86.81	342.2	207.1	306.06	74.52	106.8
61	300-305	1249	136.3	78.23	86.51	306.0	215.2	300.50	84.45	93.15
62	305-310	825	123.4	74.94	86.73	288.0	218.5	279.25	84.31	87.29
63	310-315	1337	160.1	81.25	92.23	306.5	219.0	316.13	78.85	106.4
64	315-320	1098	128.3	72.30	79.38	281.7	197.9	305.58	93.66	92.3
65	320-325	944.4	119.6	65.36	71.29	255.9	172.9	282.68	92.99	80.78
66	325-330	949.4	127.1	68.98	76.45	272.5	174.1	304.08	95.19	90.09
67	330-335	990.5	128.3	70.24	78.21	279.1	177.1	286.11	75.63	89.95
68	335-340	1043.4	131.1	71.08	77.79	285.5	191.5	329.21	100.6	98.73
69	340-345	927.5	122.1	68.15	74.34	278.3	181.8	302.21	92.12	91.01
70	345-350	1306	175.1	87.93	91.57	358.4	261.2	419.70	100.6	138.6
71	350-355	1145	139.4	78.12	82.38	340.9	214.1	327.92	97.60	103.0
72	355-360	785.4	127.9	79.97	79.07	297.2	196.4	362.19	86.61	133.4
73	360-365	971.3	129.7	69.34	71.78	298.2	193.8	345.35	95.50	114.2
74	365-370	1282	161.4	85.16	87.79	343.8	233.9	396.23	87.61	142.2
75	370-375	994.8	124.0	64.46	67.41	282.0	169.1	317.37	86.49	102.8
76	375-380	1167	141.5	71.11	73.58	289.0	191.6	356.57	96.89	115.6
77	380-385	1134	133.7	66.39	69.15	271.3	178.3	336.75	85.68	115.1
78	385-390	1335	151.2	74.59	78.85	303.7	205.4	354.40	83.63	125.0
79	390-395	1414	159.3	79.35	82.50	324.4	222.6	365.70	82.21	128.8
80	395-400	1034	132.5	75.22	76.05	299.6	188.1	347.18	76.28	123.0
81	400-405	905.8	124.5	72.30	73.98	282.7	183.6	346.67	96.04	118.4
82	410-415	682.1	116.8	68.35	67.33	254.5	165.4	336.78	94.69	114.1

Table 2 contd/...

Sr. No.	Depth (cm)	Ba	Sr	Co	V	Cu	Ni	ΣREE	Ce	Y
83	415-420	1242	131.6	71.73	73.97	293.5	194.3	328.92	90.85	108.3
84	420-425	777.6	130.8	78.64	75.54	295.0	197.0	346.26	77.54	126.3
85	425-430	863.3	138.1	80.95	77.34	290.1	197.3	374.22	79.66	139.4
86	430-435	777.2	157.4	93.81	85.12	350.5	261.6	391.00	78.34	110.1
87	435-440	873.7	148.4	94.35	88.58	359.3	233.7	368.00	84.95	131.5
88	440-445	887.3	158.3	95.08	93.50	347.5	241.8	381.33	84.98	135.6
89	445-450	939	148.6	93.36	91.91	348.2	248.2	379.31	86.47	137.3
90	450-455	936.7	160.0	94.45	95.23	340.8	241.5	383.81	90.68	131.6
91	455-460	857.5	141.3	86.26	86.92	333.7	234.8	363.19	78.37	131.2
92	460-465	1166	160.9	88.82	90.05	333.1	226.4	358.53	79.82	130.5
93	465-470	1265	166.0	93.78	94.40	345.9	246.0	410.20	89.16	127.6
94	470-475	966.7	160.6	87.50	86.54	314.8	221.4	385.94	83.54	139.1
95	475-480	958.8	153.5	84.65	86.03	303.2	214.8	365.82	82.93	125.8
96	480-485	773.3	148.2	88.99	93.44	324.6	235.3	322.37	74.86	112.7
97	485-490	1057	153.9	89.95	97.72	333.1	238.7	364.92	91.00	118.6
98	490-495	1186	163.8	99.23	108.1	355.4	314.7	398.09	104.2	124.2
99	495-500	1250	155.4	96.03	102.0	333.4	268.8	345.89	87.63	109.3
100	500-505	1170	146.7	88.68	90.64	305.8	232.9	328.64	84.27	105.4
101	505-510	988.2	149.6	94.82	93.99	314.4	234.3	334.12	81.82	114.1
102	510-515	834.8	141.2	93.29	91.84	319.5	244.5	335.84	79.20	115.4
103	515-520	1064	153.9	98.97	96.32	330.4	241.0	382.19	95.04	125.8
104	520-525	890.7	140.0	87.85	83.35	299.3	222.9	363.02	86.03	125.0
105	525-530	839.9	144.7	96.47	85.79	326.7	224.9	393.26	87.54	123.6
106	530-535	789.6	156.3	101.7	91.53	356.0	242.5	413.94	86.87	115.6
107	535-540	1078	160.4	96.98	86.41	327.8	234.6	425.31	93.40	115.5
Average		1234.4	156.7	81.7	83.0	277.1	180.4	324.0	91.7	102.1
Max		2431.0	216.0	103.0	109.8	363.8	314.7	425.3	115.4	142.2
Min		682.10	116.70	53.25	48.65	178.50	73.39	199.12	74.28	54.39

Table 3: The recovery of the major element oxides and trace elements (in % of reported values) along with the relative standard deviation (RSD) of the certified reference materials JSd-1, used in the present study. Number of replicates in each analysis is given below.

(wt %)	Reported	Analyzed	Recovery	%RSD	(mg/kg)	Reported	Analyzed	Recovery	%RSD
SiO ₂	66.5	66.54	100	7.22	Ba	520	509.6	98.0	7.35
Al ₂ O ₃	14.6	14.17	96.7	2.31	Sr	340	321.7	94.6	12.94
TiO ₂	0.64	0.64	100	0.07	Co	11.2	10.62	94.8	1.83
Fe ₂ O ₃	5.06	5.03	99.5	1.00	V	76.0	73.38	96.6	1.85
MnO	0.09	0.09	99.6	0.33	Cu	22.0	21.81	99.1	0.13
MgO	1.81	1.81	99.9	0.66	Ni	7.04	6.62	94.0	0.30
CaO	3.03	3.03	99.8	4.40	ΣREE	86.9	82.05	94.4	1.18
Na ₂ O	2.73	2.72	99.9	1.58	Ce	34.4	32.44	94.3	1.03
K ₂ O	2.18	2.17	99.2	0.40	Y	14.8	14.53	98.2	0.19
Replicates	2				3				

Table 4: Correlation coefficient matrix of (a) trace elements and ΣREEs and (b) Ti normalized trace elements and ΣREEs. Values in bold has confidence level >99%.

	Ba	Sr	Co	V	Cu	Ni	ΣREE	Ce	Y
Ba	1								
Sr	0.44	1							
Co	0.01	0.33	1						
V	0.07	0.22	0.86	1					
Cu	-0.04	-0.35	0.47	0.51	1				
Ni	-0.01	-0.36	0.30	0.38	0.91	1			
ΣREE	-0.24	0.06	0.68	0.58	0.64	0.50	1		
Ce	0.09	0.45	0.15	0.13	-0.45	-0.47	0.10	1	
Y	-0.25	-0.08	0.54	0.48	0.70	0.56	0.92	-0.15	1

(a)

	Ba/Ti	Sr/Ti	Co/Ti	V/Ti	Cu/Ti	Ni/Ti	ΣREE/Ti	Ce/Ti	Y/Ti
Ba/Ti	1								
Sr/Ti	0.66	1							
Co/Ti	0.29	0.70	1						
V/Ti	0.27	0.60	0.86	1					
Cu/Ti	0.00	-0.01	0.31	0.27	1				
Ni/Ti	-0.09	-0.23	0.03	0.06	0.86	1			
ΣREE/Ti	0.06	0.49	0.72	0.58	0.55	0.28	1		
Ce/Ti	0.46	0.83	0.51	0.38	-0.24	-0.43	0.43	1	
Y/Ti	-0.10	0.20	0.50	0.42	0.66	0.43	0.88	0.07	1

(b)

Figure captions:

- Figure 1: Map showing the sediment core location of AAS-38/4 in the Central Indian Basin, Indian Ocean.
- Figure 2: Scanning Electron Microscope (SEM) image of radiolarian index species; (a) *Collosphaeratuberosa*, (b) *Stylatractusuniversus*, (c) palagonite, (d) bubble shaped glass shard, (e) kidney shaped micronodule and (f) zeolite crystal with some radiolaria attached to it.
- Figure 3: X-ray diffractogram of clay minerals down the core AAS 38/4; (a) up to 70cm depth from core top, the main clay minerals are kaolinite+chlorite (K+C) with a minor peak of illite (I) and no smectite (S), (b) below 70cm depth, smectite appeared along with kaolinite (K), chlorite and illite and (c) below 240cm depth, smectite has the most prominent peak among all the clay minerals. Quartz peak (Q) was ubiquitous throughout the core.
- Figure 4: Biostratigraphic zonation of the core AAS-38/4 based on Quaternary radiolarian index species.
- Figure 5: (a) Sedimentation rate of the core AAS-38/4 based on the radiolarian age versus depth curve; 0-50cm depth exhibits higher sedimentation rate of 0.18cm/kyr below which it decreases down to 0.05cm/kyr and (b) $\delta^{18}\text{O}$ variation against age in kyr marking Marine Isotope Stage (MIS) 13 at the change in sedimentation rate, marked by blue thick line.
- Figure 6: Depth versus (a) biogenic silica concentration profile with the corresponding ages on the right axis and (b) Chemical Index of Alteration (CIA) values of each section of the core, indicating more intense chemical alteration in the lower part of the core.
- Figure 7: Downcore variation of trace and Rare Earth element patterns of the sediment core.
- Figure 8: Ti normalized trace and Rare Earth element patterns of the sediment core, indicating non-detrital portion of the elements.
- Figure 9: PAAS normalized REE pattern of the sediment core, showing distinct negative Ce-anomaly, positive Eu-anomaly and a middle REE enrichment.
- Figure 10: $\text{K}_2\text{O}/\text{Al}_2\text{O}_3$ ratio of the sediment sub-samples, showing a drastic decrease below the transition zone at 180-185cm, indicating change in weathering pattern from chemical to physical through time.

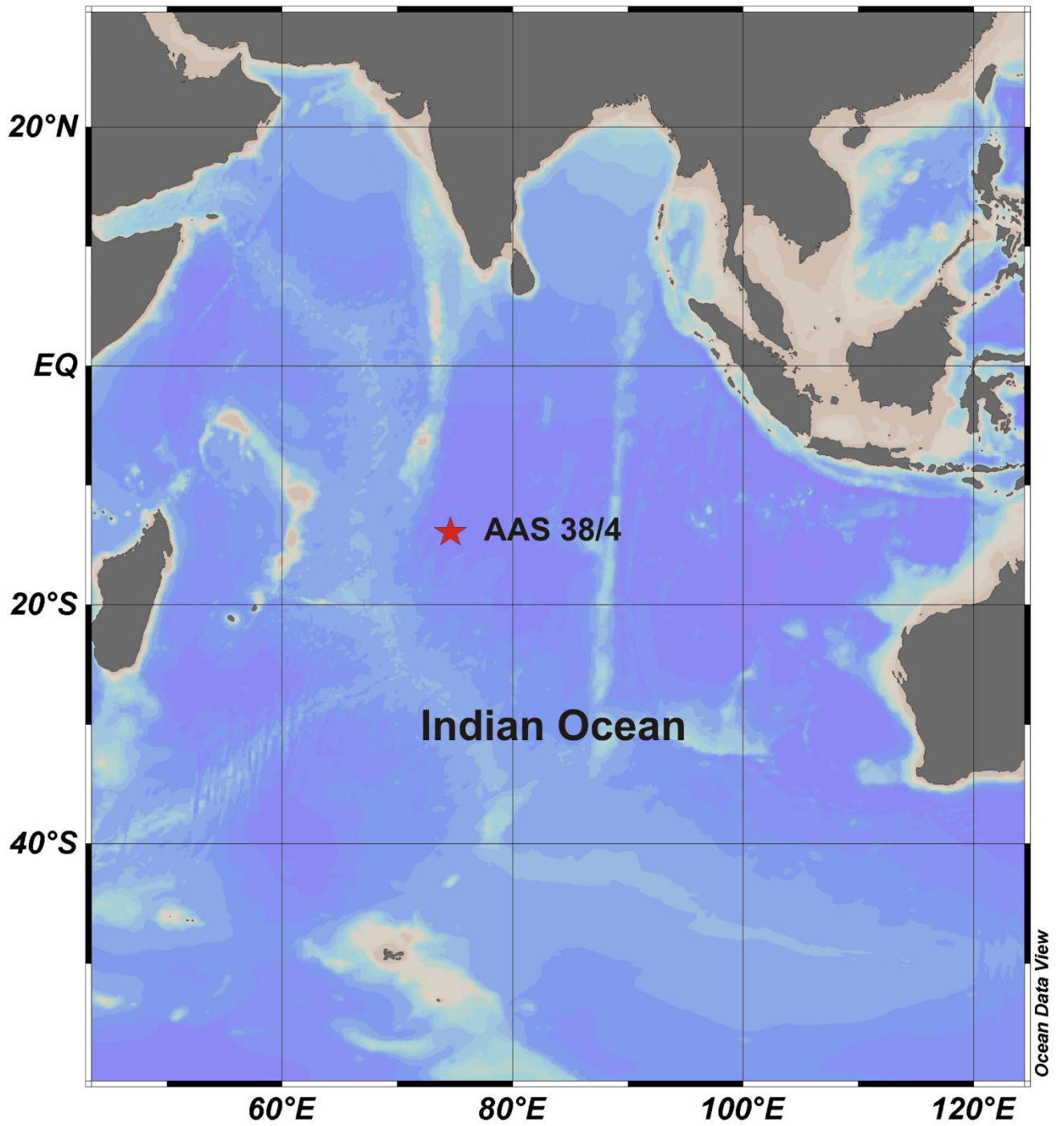
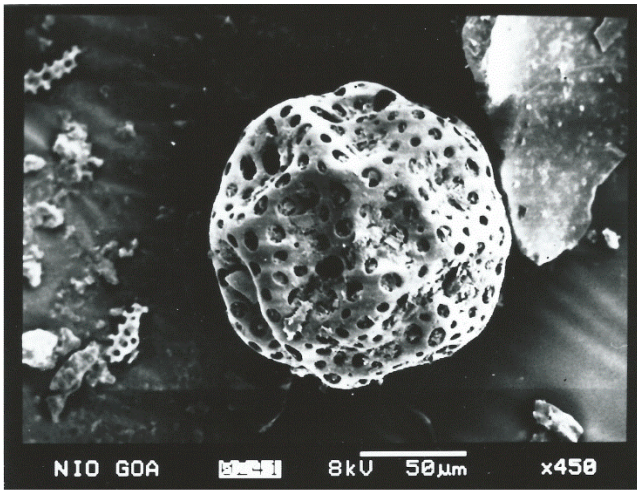
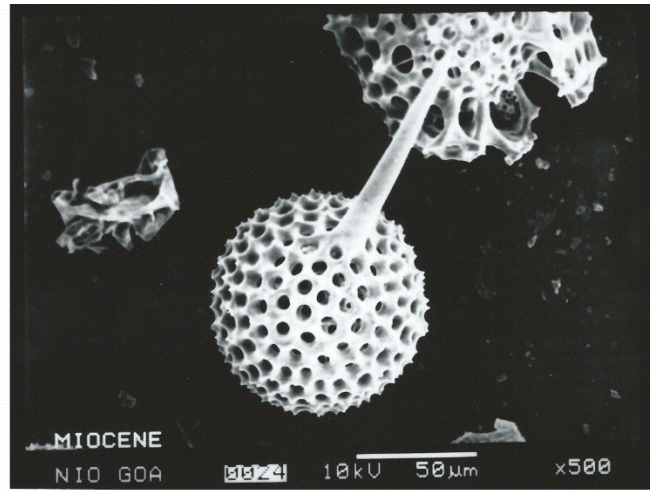


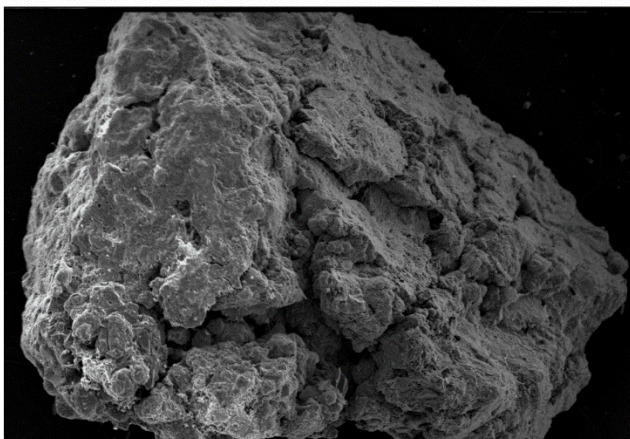
Figure 1



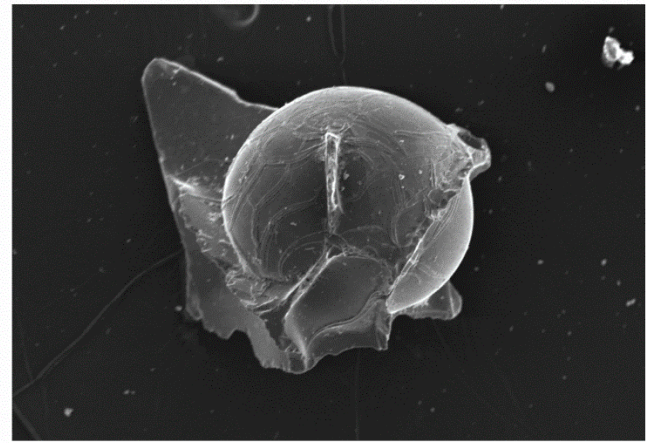
(a)



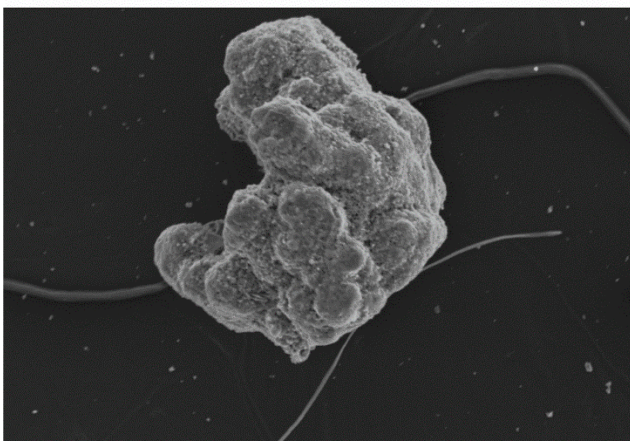
(b)



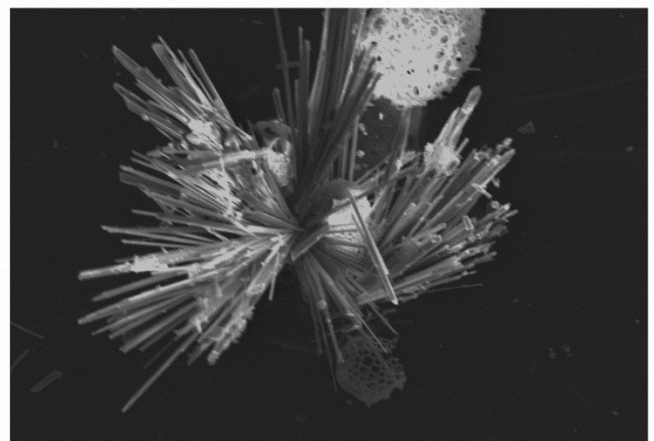
(c)



(d)

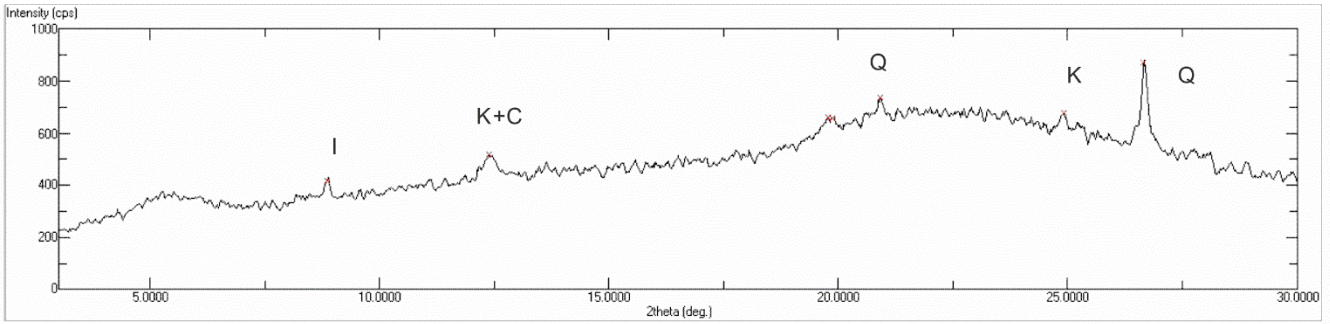


(e)

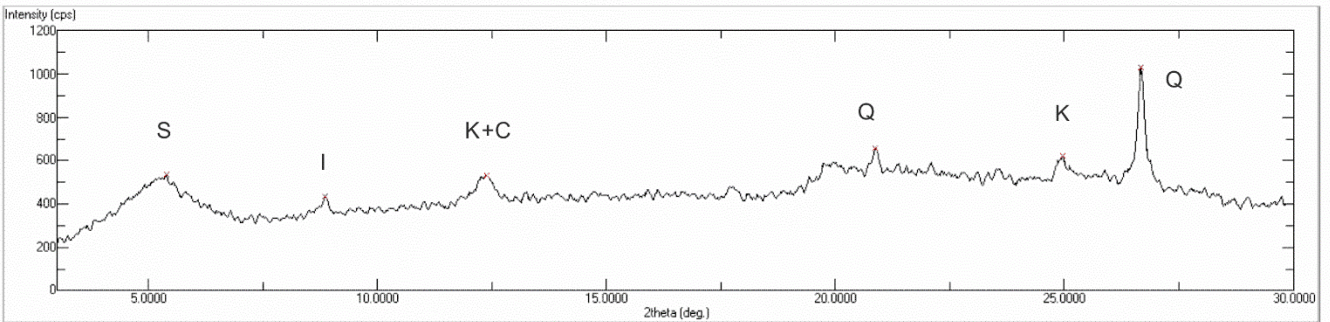


(f)

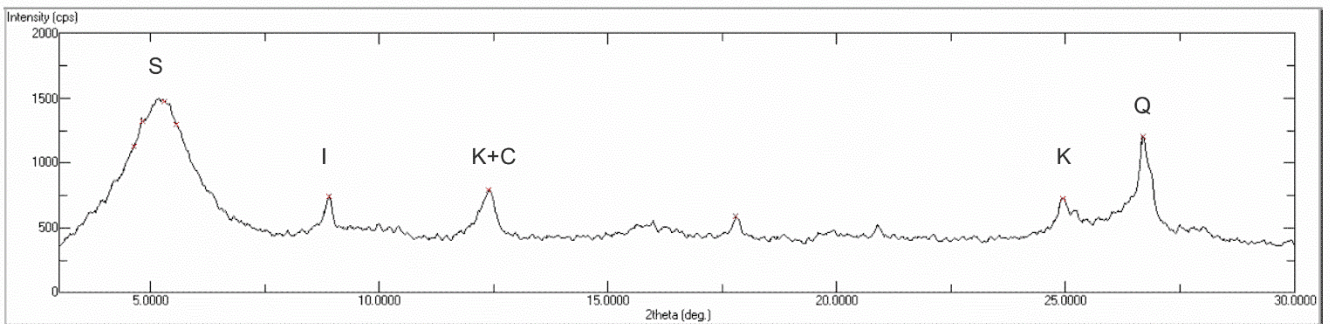
Figure 2



(a)



(b)



(c)

Figure 3

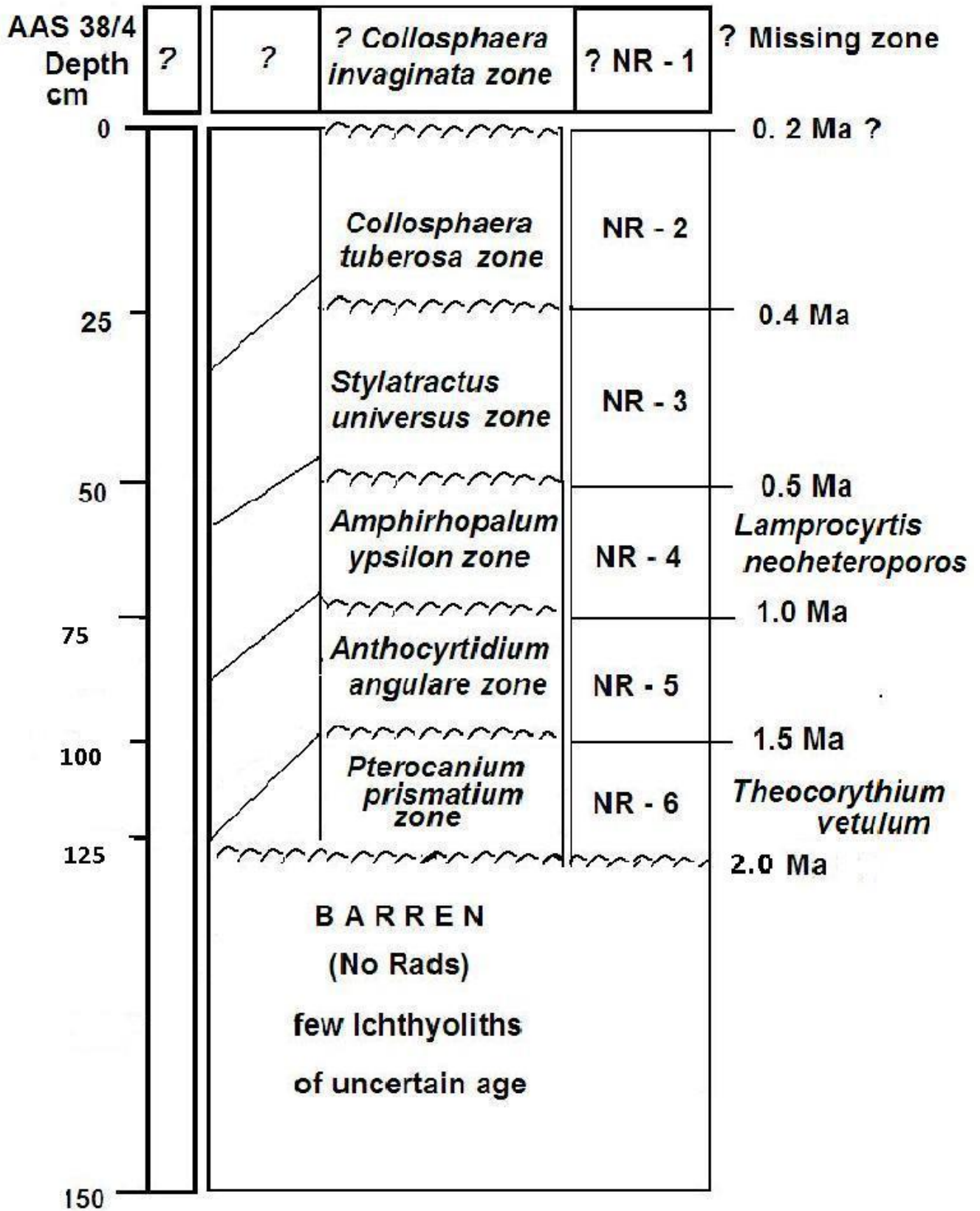


Figure 4

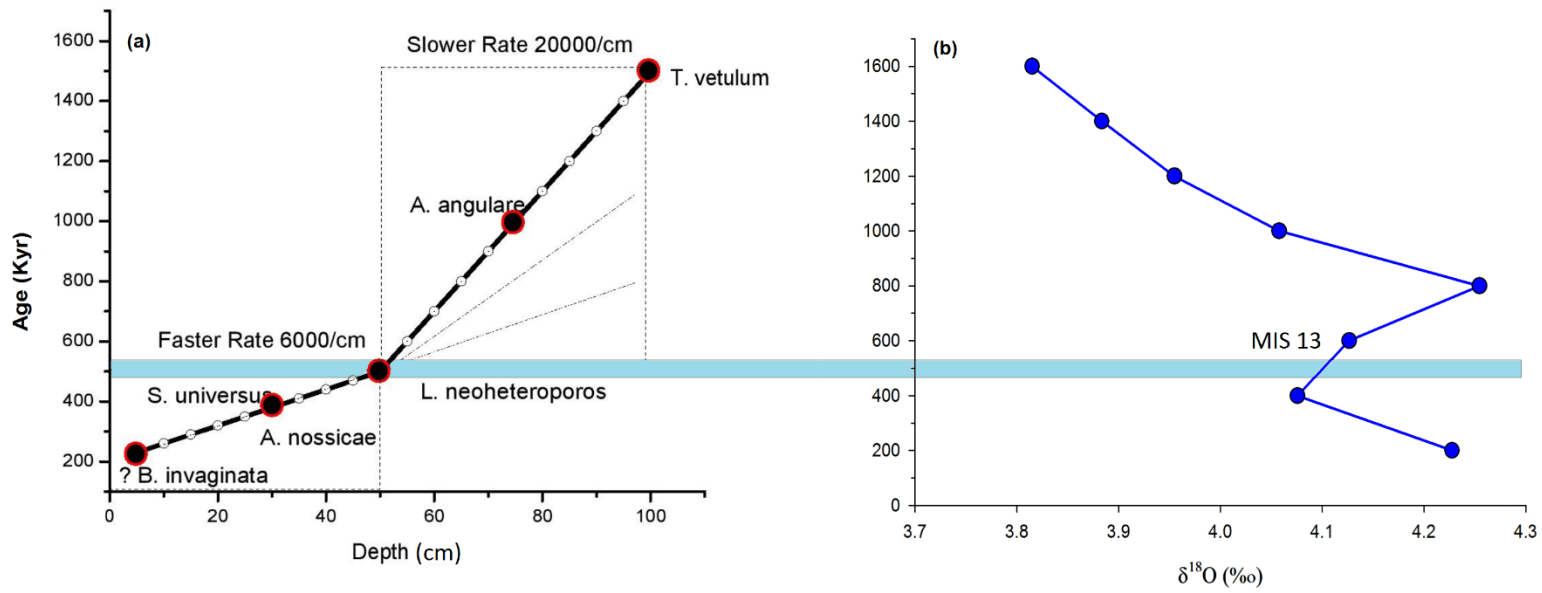


Figure 5

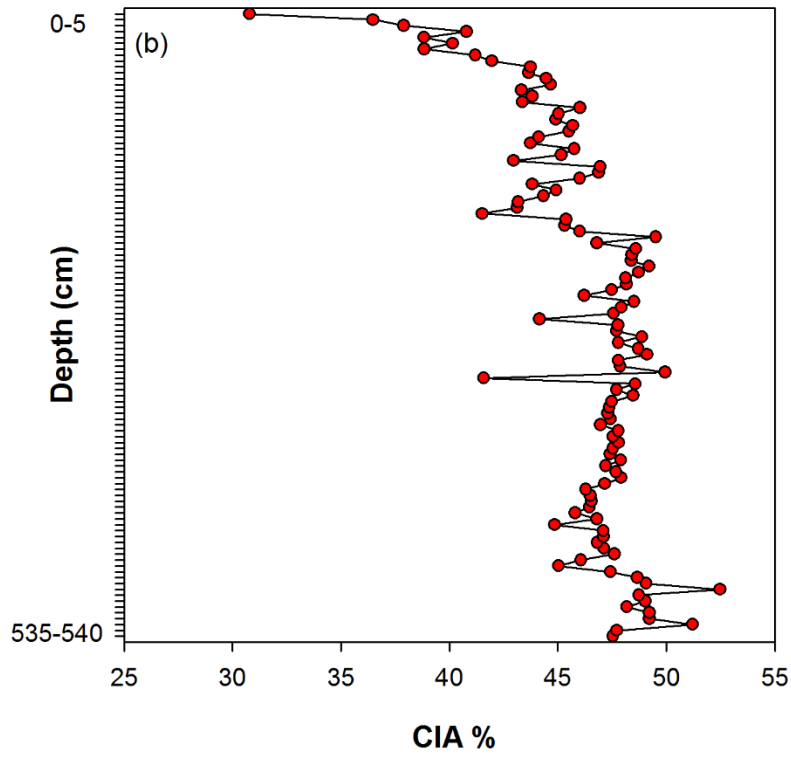
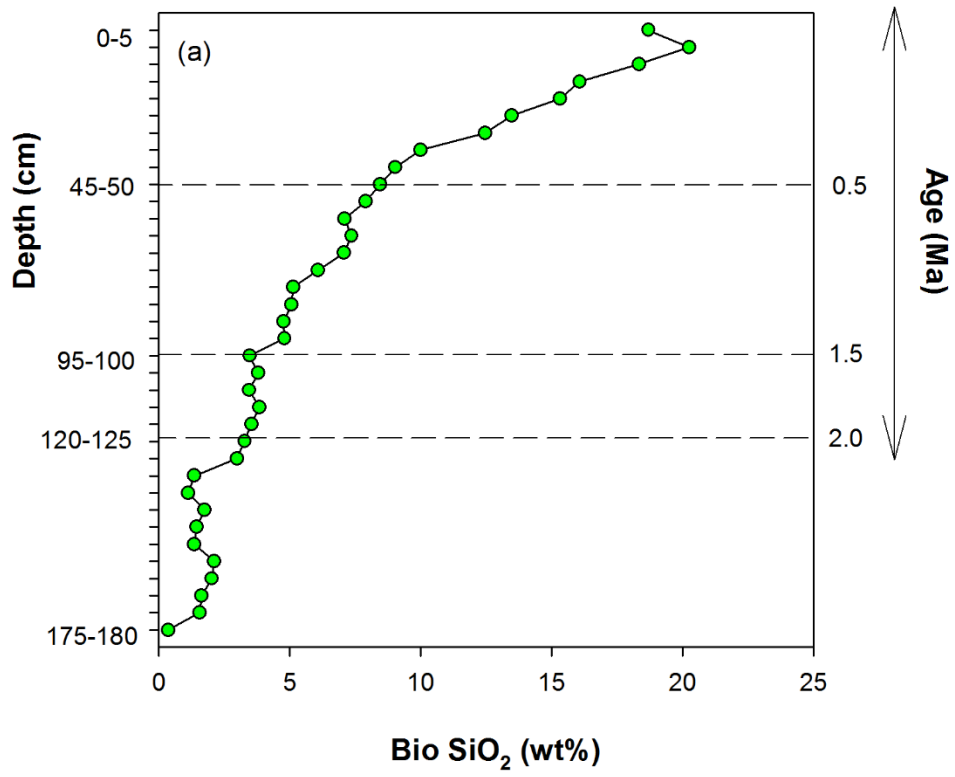


Figure 6

Figure 7

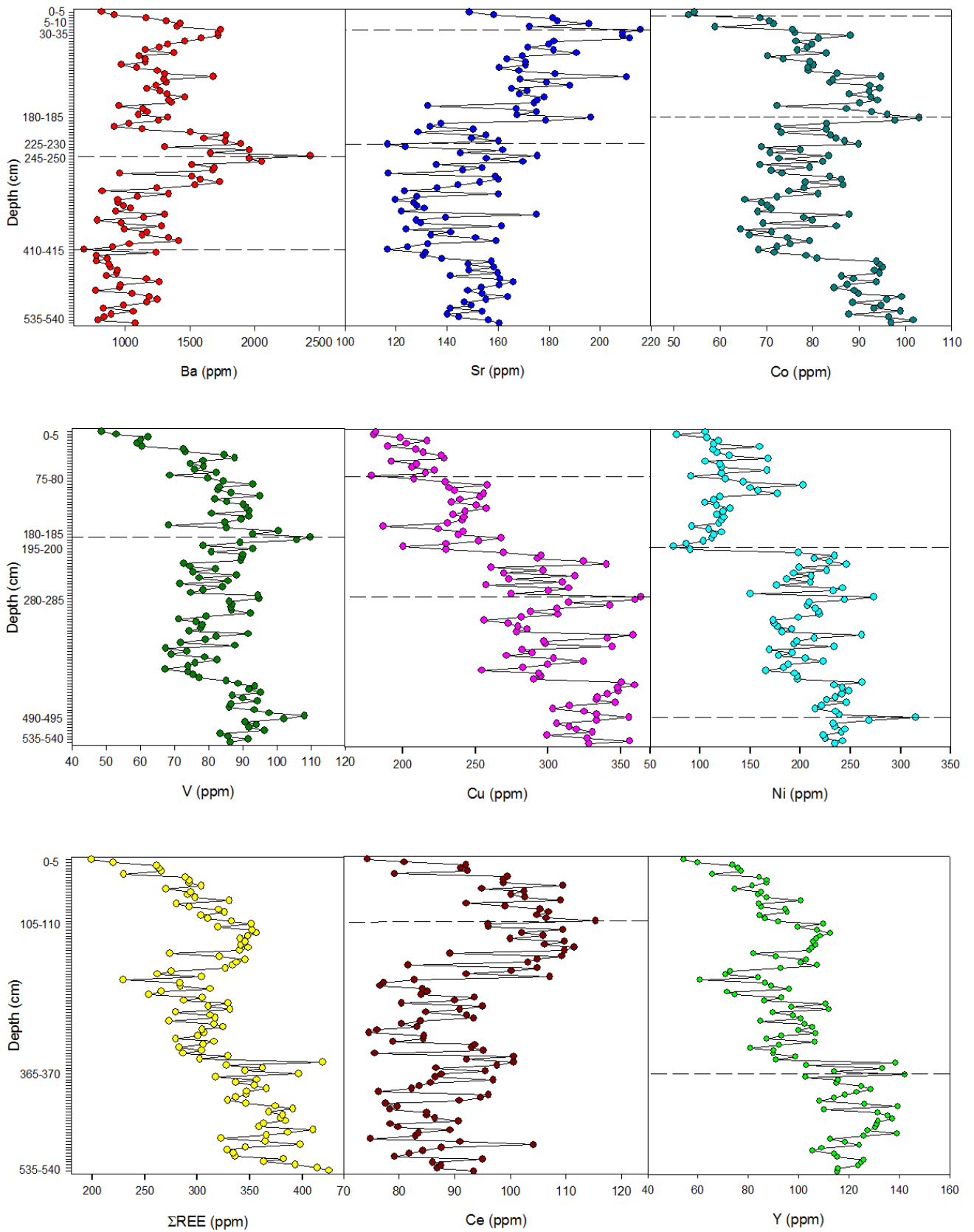
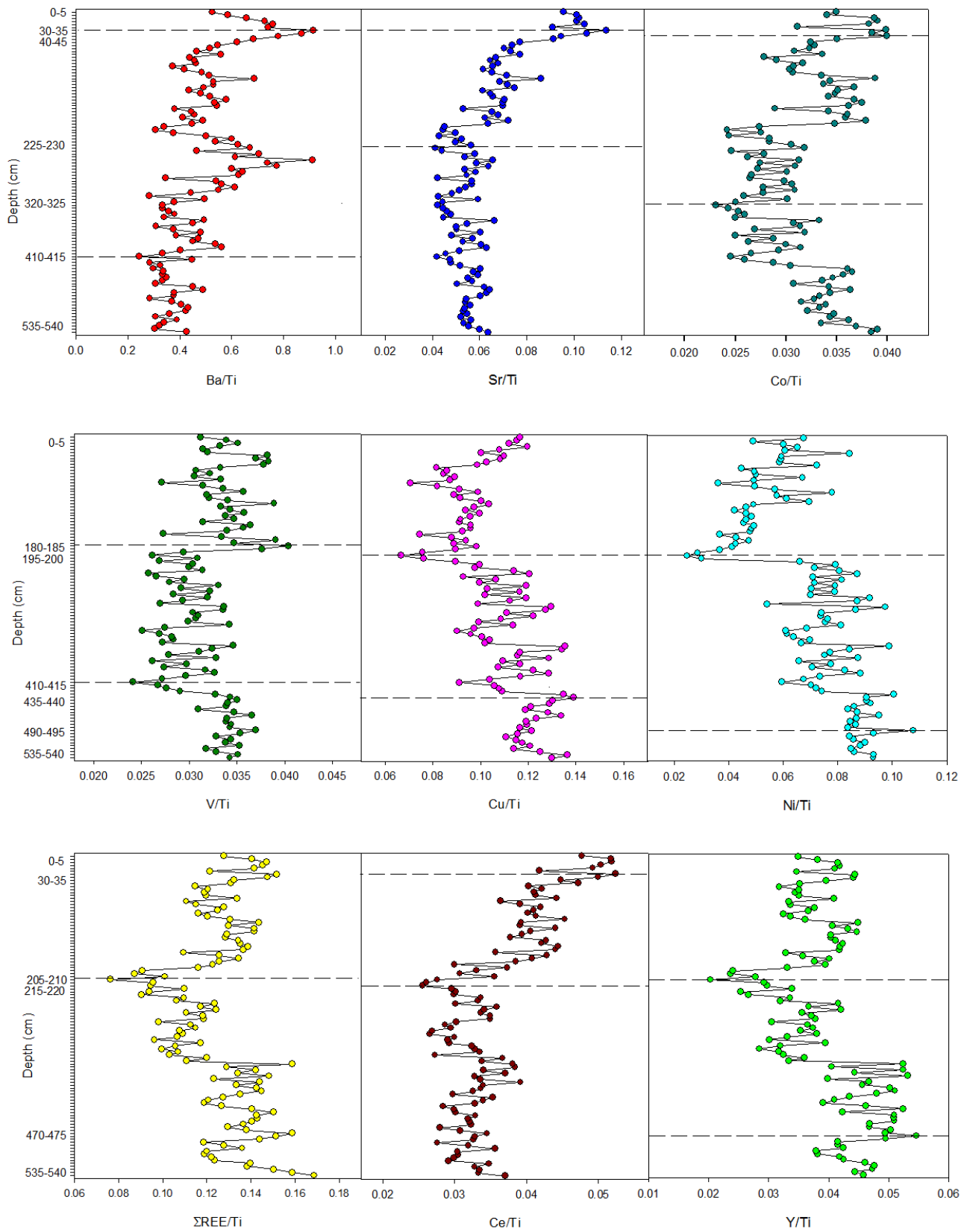


Figure 8



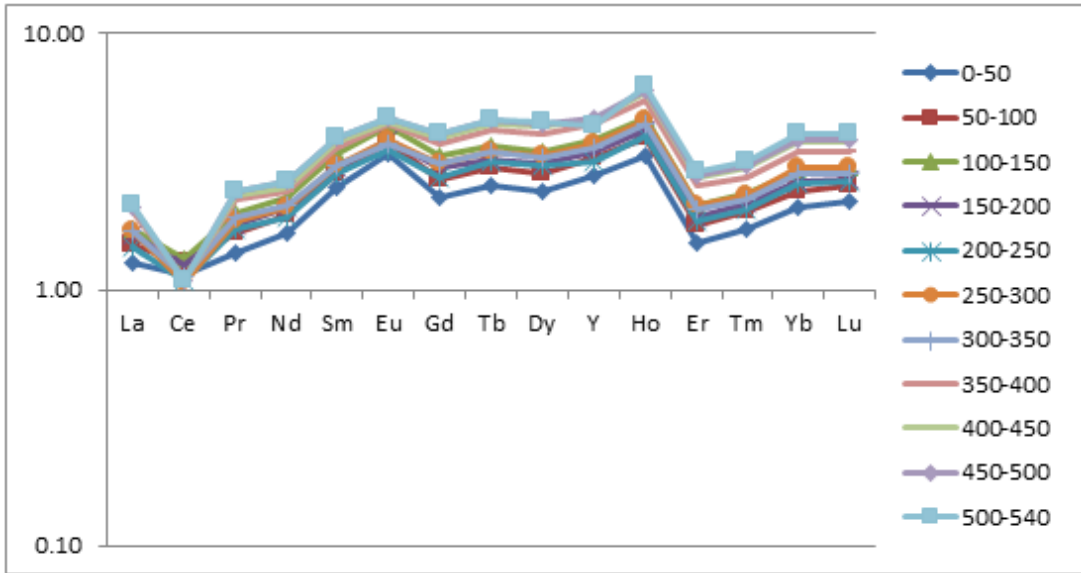


Figure 9

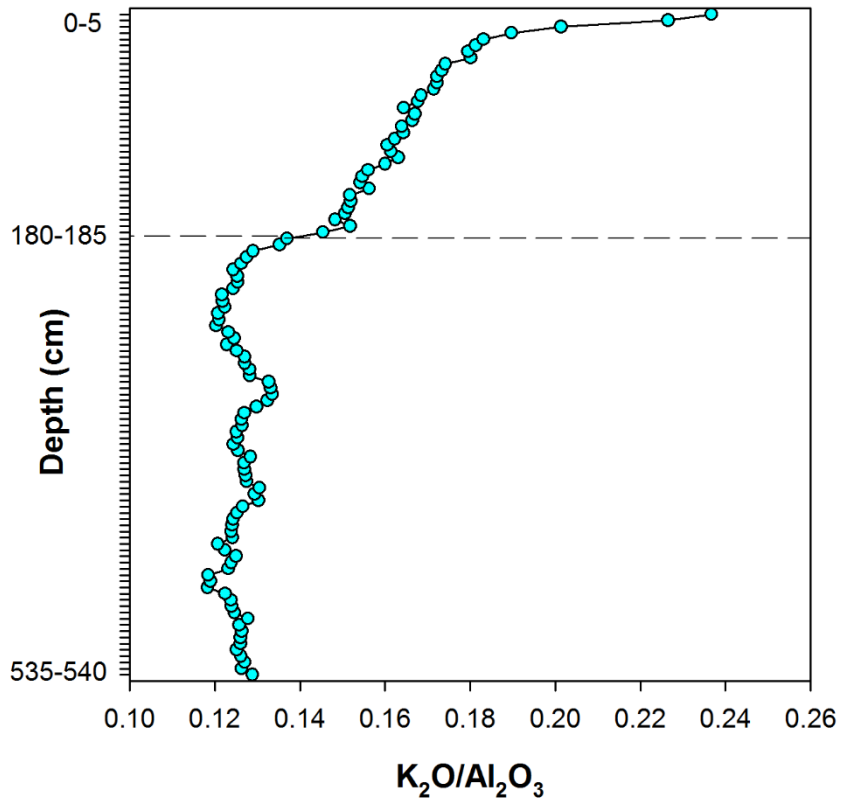


Figure 10